Differential impact of $GABA_A$ receptors and gephyrin post-translational modifications on layer 2/3 pyramidal neuron responsiveness *in vivo*

Yuan-Chen Tsai[1,2], Mohammad Hleihil[1,2], Kanako Otomo[1], Andrin Abegg[1], Anna Cavaccini[3], Patrizia Panzanelli[4], Teresa Cramer[1,2], Kim David Ferrari[1,2], Matthew J.P. Barrett[1,2], Giovanna Bosshard[1], Theofanis Karayannis[3], Bruno Weber[1,2], Jillian L. Stobart[1, 5, ¶], Shiva K. Tyagarajan[1,2, ¶,*]

[1]*Institute of Pharmacology and Toxicology, University of Zurich, Winterthurerstrasse 190, 8057 Zurich, Switzerland*

[2]*Center for Neuroscience Zurich (ZNZ), Winterthurerstrasse 190, 8057 Zurich, Switzerland*

[3] *Brain Research Institute, University of Zurich, Winterthurerstrasse 190, 8057 Zurich, Switzerland*

[4] *Department of Neuroscience Rita Levi Montalcini, University of Turin, Turin, Italy*

[5] *College of Pharmacy, University of Manitoba, Winnipeg, MB R3E 0T5*

¶ co-senior, equal contribution

*Corresponding author
tyagarajan@pharma.uzh.ch

Running Title: GABAergic inhibition facilitates sparse sensory encoding

Key points:

- While GABAergic inhibition from interneuron subtypes regulates cortical microcircuit activity the molecular determinants have remain unclear.
- We demonstrate that specific-$GABA_A$ receptor subtypes contribute differentially to layer 2/3 neuronal activities in mouse barrel cortex.
- Importantly, we link the GABAAR contributions to the scaffolding properties of its important postsynaptic density protein gephyrin. We show that different PTMs on gephyrin determines neuronal excitability via GABAAR recruitment and modulation of inhibition within layer 2/3 neurons.
- Specifically, α1 and α2 subunits containing $GABA_A$ receptors, along with their scaffolding protein gephyrin determine the distribution of high, medium and low activity pyramidal neurons during sensory encoding, whereby controlling the total activity of cortical microcircuit.

Key words: signal transduction, barrel cortex, cortical microcircuit, inhibition, interneurons.

Abstract

A diverse set of $GABA_A$ receptors ($GABA_ARs$) enable synaptic plasticity adaptations at inhibitory postsynaptic sites in collaboration with the scaffolding protein gephyrin. Early studies helped to identify distinctions between $GABA_AR$ subtypes allocated within specific functional circuits, but their contribution to the changing dynamics of a microcircuit remains unclear. Here, using the whisker-barrel system in mouse, we assessed the contribution of specific synaptic $GABA_AR$ subtypes and gephyrin scaffolding changes to sensory processing *in vivo*. We monitored spontaneous and evoked Ca^{2+} transients in layer 2/3 pyramidal cells with the genetically encoded Ca^{2+} sensor RCaMP1.07. Using *Gabra1* or *Gabra2* global and conditional knockout mice, we uncovered that α1- and α2-$GABA_ARs$ determine the sparseness of L2/3 pyramidal neuron encoding. In a cell-type dependent manner, α1-$GABA_ARs$ and α2-$GABA_ARs$ affected neuronal excitability and the reliability of neuronal responses after whisker stimulation. We also discerned that gephyrin with its diverse post-translational modifications (PTMs) shows preference for specific $GABA_AR$ subtype to facilitate microcircuit activity. Our results underscore the relevance of the diversity of $GABA_ARs$ within a cortical microcircuit.

Introduction

The primary somatosensory cortex (S1) is composed of excitatory and inhibitory neurons that encode passive sensory experience, training on sensory tasks, and sensory perceptual learning (Feldman and Brecht 2005). Sensory information is processed in a selective manner and is encoded sparsely. The rodent whisker system is a well-established model to study how sensory perception is encoded within organized barrel cortex columns. A whisker deflection leads to depolarization in the majority of neurons, but only around 10% of these neurons respond with action potentials (Crochet et al. 2011). In layer 2/3 (L2/3) of the barrel cortex, the excitability of a cortical microcircuit is tightly modulated by inhibitory interneurons (Kapfer et al. 2007). The excitatory neurons outnumber GABAergic interneurons within the neocortex, although precise numbers vary across different cortical areas and layers. Despite this disparity in excitatory and inhibitory neuron numbers, the probability of finding excitatory-excitatory connections between 2 pyramidal neurons in supragranular layers is relatively low, whereas the connectivity between pyramidal cells and inhibitory interneurons is much higher (Holmgren et al. 2003; Lefort et al. 2009; Avermann et al. 2012; Petersen 2019). Hence, GABAergic interneurons play a crucial role in controlling the activity of the pyramidal neurons within a cortical microcircuit in the superficial layers.

At the postsynaptic sites, $GABA_A$ receptors ($GABA_ARs$), its main scaffolding protein, gephyrin, and their associated signaling proteins facilitate downstream signal transduction to modulate pyramidal cell excitability. The importance of GABA for cortical plasticity has been reported for the barrel cortex function, while the molecular mechanisms underlying plasticity changes at GABAergic synapses remain unclear. A local infusion of the $GABA_AR$ antagonist gabazine leads to increased spontaneous depolarization of L2/3 pyramidal neurons (Gentet et al. 2010). $GABA_ARs$ are assembled from a heterogeneous gene pool to form pentameric ion channels. These $GABA_AR$ subtypes that constitute the $GABA_AR$ pentamers also exhibit

distinct expression patterns within a given brain circuit (Fritschy and Panzanelli 2014). $GABA_AR$ subtypes are also uniquely localized within different cortical layers. The α1 subunit-containing $GABA_ARs$ (α1-$GABA_ARs$) are more uniformly distributed across all six cortical layers, whereas the α2 subunit-containing $GABA_ARs$ are abundantly expressed in the supragranular layers (layer 1, 2 and 3), and the α3 subunit containing-$GABA_ARs$ are more abundant in layers five and six (Fritschy and Mohler 1995). Hence, this spatial segregation of $GABA_AR$ subtypes implies that distinct functional roles exist for $GABA_AR$ subtypes within the somatosensory cortex.

$GABA_AR$ synaptic localization is facilitated by diverse receptor-interacting proteins that include neuroligin-2 (Fritschy, Panzanelli, and Tyagarajan 2012), collybistin (deGroot et al. 2017; Hines et al. 2018), and gephyrin (Tyagarajan and Fritschy 2014). Among these proteins, gephyrin is unique because it aids activity-dependent adaptations at GABAergic synapses over different time scales (Battaglia et al. 2018). Many signaling pathways converge onto the gephyrin scaffold and in turn induce various post-translational modifications (PTMs) on gephyrin (Zita et al. 2007; Kuhse et al. 2012; Dejanovic and Schwarz 2014; Dejanovic et al. 2014; Ghosh et al. 2016). Super-resolution microscopy studies of gephyrin PTM mutants have shown that compaction of gephyrin molecule and synaptic dwell time of α2 subunit-containing $GABA_ARs$ contribute to activity-dependent adaptation (Flores et al. 2015; Battaglia et al. 2018). However, *in vivo* functional significance of gephyrin PTMs on $GABA_AR$ synapse recruitment and plasticity remains unexplored.

The barrel cortex function is facilicated by GABAergic inhibition via interneuron networks that coordinate pyramidal neuron activity during sensorimotor behavior (Petersen 2014). At the microcircuit level, parvalbumin-expressing (PV+) neurons that typically synapse onto pyramidal cell soma and proximal dendrites become activated during passive and active whisker sensing. In contrast, somatostatin-expressing (SOM+) interneurons that typically

synapse onto distal dendrites of a pyramidal cell become hyperpolarized during whisker sensing (Gentet et al. 2012). The importance of inhibition is even more prominent in awake mice as the cortical state changes from quiet to active whisker behavior involves the reorganization of GABAergic neuronal network activity (Gentet et al. 2010). The response of pyramidal neurons to different interneuron inputs during sensory processing relies heavily on the downstream receptor complex and postsynaptic density proteins. Hence, within a cortical microcircuit, differential $GABA_AR$ activation within the principal cell must contribute to encoding and regulating sensory inputs. Currently, the identities of specific $GABA_ARs$ and the role of scaffolding proteins in determining cortical microcircuit functional specificity are unknown.

In this study, we examined the involvement of two major $GABA_AR$ subtypes, namely α1-$GABA_AR$ and α2-$GABA_AR$, and gephyrin PTMs, for sensory input-dependent cortical microcircuit function. In this regard, we employed a genetically encoded Ca^{2+} sensor, RCaMP1.07, to measure Ca^{2+} transients in L2/3 pyramidal neurons in the barrel cortex in wild-type (WT) and *Gabra1* or *Gabra2* global and conditional gene-deficient mice. We report α1- and α2- containing $GABA_AR$ subtypes, together with their scaffolding protein gephyrin, facilitate sparse encoding of whisker stimulation-induced sensory response within L2/3 pyramidal neurons. We identify that at a global and a local level, α1-$GABA_ARs$ and α2-$GABA_ARs$ determine the excitability of L2/3 pyramidal neurons in the opposite manner. Specifically, within L2/3 pyramidal cells, α1 and α2- $GABA_ARs$ control sparseness within the responding population. Importantly, distinct gephyrin PTM facilitates inhibitory synapse plasticity via the recruitment of either α1- or α2-containing $GABA_ARs$ to synaptic locations. This dynamic process helps fine-tune L2/3 pyramidal neuron excitability. Together, the changing needs of the barrel cortex L2/3 microcircuit during sensory stimulation are facilitated by specific $GABA_AR$ subtypes and diverse gephyrin PTMs.

Methods

All experiments were performed in accordance with the European Community Council Directives of November 24, 1986 (86/609/EEC) and approved by the cantonal veterinary office of Zurich.

Animals

Male and female mice C57BL/6J were purchased (Charles River, Germany), and the following strains were maintained in house: FVB, *Gabra1* KO (Vicini et al., 2001), *Gabra2* KO (Panzanelli et al., 2011; Koester et al., 2013), *Gabra1*$^{flox/flox}$ (Vicini et al., 2001), *Gabra2*$^{flox/flox}$ (Duveau et al., 2011). Control groups were sex-matched with the experimental groups. They were group-housed in an inverted 12-hour light/dark cycle. All mice underwent surgery at 8-12 weeks of age and were imaged repeatedly (2-4 times per week) under a 2-photon microscope for up to 5 months.

Cloning and virus production

The AAV2/6-CaMKIIa-RCaMP1.07 construct was generated by cloning of the RCaMP1.07 gene (Ohkura et al., 2012; Pilz et al., 2015) into an adeno-associated plasmid backbone (AAV2) under a calcium/calmodulin dependent protein kinase II alpha (CaMKIIα) promoter.

The eGFP-gephyrin-K148R, eGFP-gephyrin-DN, eGFP-gephyrin S303/305A expression vectors have been described previously (Flores *et al*., 2015; Ghosh *et al*., 2016), and were subcloned into an AAV2 plasmid backbone containing the human synapsin1 (hSyn1) promoter, in an inverted orientation, and flanked by 2 different loxP sites. The transgene was packaged into AAV 6 serotype. All the AAV6 recombinant viruses were generated by the Viral Vector Core at the University of Zürich. AAV2/6-CaMKIIa-CreER^{T2} virus was purchased from Vector Biolabs (#2014-1208).

196 ***Lateral ventricle viral injection***

197 C57BL/6 mouse pups received bilateral viral injection into lateral ventricle at post-natal day 0
198 (P0) (Kim et al. 2013). In short, P0 pups were briefly anaesthetized with isoflurane, and 2 µl
199 viral solution per lateral ventricle was injected using a 10 µl Hamilton syringe with a 32 gauge.
200 Lateral ventricles were targeted using bregma and lambda as reference points to draw the mid-
201 line, the needle was inserted into a site 1 mm lateral from the mid-point of the mid-line
202 perpendicular to the skin surface. The needle was inserted to a depth of 3 mm into the skull to
203 ensure injection into the lateral ventricle. Virus used for the experiments was AAV8-CaMKIIa-
204 tdTomato in the control and experimental groups. The injected pups were placed back in their
205 home cage after waking up from anesthesia. The mice were housed under normal conditions
206 until 2-months of age when they were then used for experiments.

207

208 ***Tamoxifen administration***

209 Tamoxifen (1 mg per animal; Sigma, T5648) was given intraperitoneally (i.p.) for 4
210 consecutive days to induce Cre recombinase activity from $CreER^{T2}$. The neurons expressing
211 the transgene were imaged 5-7 days post final tamoxifen injection.

212

213 ***Surgery and virus injections for 2-photon Ca^{2+} imaging***

214 Surgical procedures were divided into 2 steps, which were 2-4 days apart. In the first surgery,
215 after fixing the mouse head in a stable position in a stereotaxic frame, an incision was made
216 along the mid line to expose the skull. After cleaning the bone, bonding reagent (ONE COAT
217 7 Universal, Coltene) was applied, and then a head cap was created using layers of light-cured
218 dental cement (SYNERGEY D6 Flow, Coltene). Finally, the custom-made aluminium head
219 post was attached to the head cap. These procedures were carried out under isoflurane (4% for
220 induction and 1.5-2% for maintenance, Forene, AbbVie). The second surgery involved a

craniotomy, cortical viral injection and chronic window implantation. With a dental drill, a small piece of skull was removed above the sensory cortex to expose the barrel cortex. A glass pipette and hydraulic pump were used to inject 150 nL of virus (injecting speed 50-70 nL per minute) at a depth of 350 μm beneath the brain surface into the whisker areas identified by Intrinsic optical imaging (see below). Immediately after the injections, a 3x3 mm coverslip was fixed right above the exposed brain and secured with dental cement to the head cap. Buprenorphine (Temgesic 0.1 mg/kg) was given before and after surgical procedures for 3 days.

Intrinsic optical imaging (IOI)

IOI was used to identify barrel areas of the corresponding whiskers in the left somatosensory cortex. This technique was used to image activation of barrel areas through the skull (before craniotomy) to map the whisker field for potential viral injections, and through the cranial window to map specific whisker areas before 2-photon imaging. Under a red light (630 nm illumination), the activated brain region (imaged 400 μm under cortical surface) was identified by increased light absorption following whisker deflection by a piezo stimulator. Imaging was done by using a 12-bit CCD camera (Pixelfly VGA, PCO imaging), and the animals were maintained under 1-1.2% isoflurane.

Two-photon imaging

A custom-built 2-photon laser-scanning microscope (Mayrhofer et al. 2015) with a 20x water immersion objective (W Plan-Apochromat 20x/1.0 DIC VIS-IR, Zeiss) was used for *in vivo* Ca^{2+} imaging in anaesthetized mice. The microscope was equipped with a Ti:sapphire laser (Mai Tai; Spectra-Physics) set to 1040 nm to excite RCaMP1.07. Fluorescence emission was detected with GaAsP photo-multiplier modules (Hamamatsu Photonics) fitted with a 520/50

nm band pass filter or a 607/70 band pass filter and separated by 560 nm dichroic mirror (BrightLine; Semrock). A customized version of ScanImage (r3.8.1; Janelia Research Campus) was used for setting imaging parameters and to control the microscope.

Confirmation of viral expression at the injected site and neuronal activation during whisker stimulation was examined first, before the series of imaging sessions. Every imaging session comprised 40 trials of spontaneous activity and 40 trials with whisker deflection (90 Hz, 1 s, piezo-based stimulator), while the duration of each trial was 15 s. Fast images were taken (11.84 Hz, 128x128 pixels) to capture neuronal Ca^{2+} responses. Imaging depth ranged from 160-200 μm beneath the cortical surface, which was in layer 2/3 of the barrel cortex. Once a field of view was selected, the same field was imaged for 3-4 sessions on different days, and an extra 3 sessions if the animals were subjected to tamoxifen injections.

Western Blot analysis

Barrel cortices from both hemispheres were isolated surgically and lysed mechanically in EBC lysis buffer (50 mM Tris-HCl, 120 mM NaCl, 0.5% NP-40, and 5 mM EDTA) containing a protease inhibitor cocktail (cOmplete™, Mini Protease Inhibitor Cocktail, Roche) and phosphatase inhibitors (Phosphatase Inhibitor Cocktail 2, Phosphatase Inhibitor Cocktail 3, Sigma-Aldrich), and then incubated for 1 hour on ice. The lysates were then centrifuged at 23,000 rpm (~48,500 rcf) for 30 minutes. Samples were prepared for loading by mixing 30 μg of protein in 5xSDS sample buffer containing 15% 2-Mercaptoethanol (Bio-Rad) and heated at 90 °C for 5 minutes. Then samples were loaded onto 8% SDS-polyacrylamide gels and run in Tris-glycine buffer at room temperature. Gels were transferred to a PVDF membrane. The membranes were blocked for 1 hour at room temperature with 5% blocking agent (Roche Diagnostic) in TBST (100 rpm shaker). Primary antibodies in blocking solution were then added to the membrane and incubated overnight at 4 °C (100 rpm shaker). After washing with

TBST, the membranes were then incubated for 1 hour at room temperature with secondary antibodies coupled to either horseradish peroxidase or IRDye® (LI-COR) to visualize the protein bands with either film (FujiFilm) or Odyssey imager (LI-COR). Intensity of the bands were quantified using ImageJ. The levels of GABRA1, GABRA2 and GABRA3 were normalized to actin levels.

Immunohistochemistry

All mice were perfused with ice cold artificial cerebrospinal fluid (ACSF; in mM: 125 NaCl, 2.5 KCl, 1.25 NaH_2PO_4, 26 $NaHCO_3$, 25 D-glucose, 2.5 $CaCl_2$, and 2 $MgCl_2$), which was oxygenated (95% O_2, 5% CO_2) for 30 minutes. After isolating the brains, the tissues were subjected to 90 minutes post fixation in 4% paraformaldehyde (PFA) at 4˚C. The post-fixed brain was left overnight in 30% sucrose at 4˚C for cryo-protection. The frozen brains were cut into 40 µm thick coronal sections by using microtome and stored in anti-freeze buffer. Sections within the coverage of the barrel field were selected and stained for the α1 or α2 $GABA_AR$ subunit (see antibody list) and an appropriate secondary antibody was used to visualize the receptor localization. The images (1024x1024 pixels) were captured using a confocal LSM 700 microscope (Zeiss) and synaptic clusters were analysed using ImageJ image-processing plugin (github repository: https://github.com/dcolam/Cluster-Analysis-Plugin). Z-stack images were taken to cover the cell body and its apical dendrite, and these images were then collapsed into 2D images for cluster analysis. Auto-thresholding moments method was applied. A mask over the somatic region was created for every analysed neuron (10-15 neurons per mouse, 4-5 mice per group) and the mask was enlarged by a factor of 1. Colocalization analysis was then performed for GABRA1 or GABRA2 staining. GABRA1 or GABRA2 particles were identified if the sizes fell within the range between 0.03 µm and 5 µm. Imaging and image processing were performed under blinded condition.

296 ***Slice preparation***

297 For miniature inhibitory postsynaptic current (mIPSC): 4 weeks old mice were injected in the
298 barrel cortex with the described virus. After another 4 weeks, mice were sacrificed by cervical
299 dislocation followed by decapitation under anaesthesia. The brains were removed quickly and
300 immersed in ice-cold cutting solution (in mM): 110 sucrose, 60 NaCl, 3 KCl, 1.25 NaH2PO4,
301 28 NaHCO3, 0.5 CaCl2, 7 MgCl2, 5 D-glucose. The slices were incubated at 32˚C for >30
302 minutes in ACSF, in mM: 125 NaCl, 2.5 KCl, 1.25 NaH2PO4, 26 NaHCO3, 25 D-glucose, 2.5
303 CaCl2, and 2 MgCl2. 300 µm coronal slices of the virus-injected area of the somatosensory
304 cortex were made using a Leica VT1200 vibratome (Leica). After the recovery period, slices
305 were maintained at RT with continuous perfusion of carbogenated ACSF (95% O2, 5% CO2).
306 All recordings were performed at RT.

307 For evoked inhibitory postsynaptic current (eIPSC): virus were stereotactically injected
308 into the L2/3 barrel cortex of 6-8 weeks old mice. After allowing 4 weeks of virus expression,
309 mice were anaesthetized with isoflurane and sacrificed by decapitation and their brains were
310 rapidly harvested and transferred to ice-cold dissecting solution containing (in mM): 110
311 choline chloride, 35 MgCl2, 25 D-glucose, 25 NaHCO3, 12.5 KCl, 6.25 NaH2PO4, 0.5 CaCl2,
312 saturated with 95% O2 and 5% CO2. 270 µm coronal slices containing barrel cortex were
313 sectioned using a Vibrotome VT 1200S (Leica) then transferred to ACSF containing (in mM):
314 115 NaCl, 35 KCl, 25 NaHCO3, 25 D-glucose, 12 NaH2PO4, 2 CaCl2, 1.3 MgCl2,
315 continuously aerated with 95% O2 and 5% CO2. Slices were kept at RT and recovered in ACSF
316 for at least 30 minutes before recording.

317

318 ***Electrophysiology***

319 For mIPSC: Recordings were amplified by Multiclamp 700B amplifier and digitized with
320 Digidata 1440 (Molecular Devices). The recording electrode was pulled from a borosilicate

glass pipette (3–5 MΩ) using an electrode puller (PC-100, NARISHIGE Group). Pipettes were filled with caesium-based solution containing (in mM): 120 CsCl, 10 EGTA, 10 HEPES pH 7.4, 4 MgCl2, 0.5 GTP and 2 ATP. Events were isolated by adding CNQX (25 µM, Merck), AP-5 (50 µM, almone labs) and tetrodotoxin (1 µM, Affix Scientific). 10 min after establishing the whole-cell mode, mIPSCs were analysed for a duration of 2 min. Events were recorded using Clampex 10.7 software (Molecular Devices). Recordings were filtered offline using a Bessel low pass filter at 500 Hz (Clampfit 10.7, Molecular Devices) and analysed using MiniAnalysis 6.0.7 software (Synaptosoft). Data were analyzed by ordinary One-way or Brown-Forsythe and Welch One-way ANOVA followed by Tukey's or Dunnet T3 multiple comparison tests, respectively.

For eIPSC: Slices were placed in the recording chamber of an upright microscope (Axioscope 2 FS, Zeiss) kept at 28.9°C, superfused with ACSF at a rate of 2 ml/min and continuously oxygenated with 95% O2 and 5% CO2. Whole-cell, voltage clamp experiments were performed using borosilicate patch pipettes (1.5 OD X 0.86 ID X 75 L mm, Harvard Apparatus), pulled with a DNZ Universal Electrode Puller (Zeitz-Instruments) to have a resistance of 3-4 MΩ and filled with a solution containing (in mM): 130 CsMeSO3, 10 HEPES, 5 CsCl, 5 NaCl, 2 MgCl2, 2 EGTA, 0.4 GTP, 0.1 EGTA, 0.05 CaCl2 (pH 7.3, 280-290 mOsm/kg). Each cortical pyramidal neuron was voltage-clamped at 0 mV during the recording. IPSCs were evoked by stimulation through a borosilicate glass pipette filled with ACSF, which was connected to a constant current stimulator (Stimulus Isolator Model IS4, Primelec) and placed within 150 µm from the soma of the recorded neuron. A stimulus of increasing amplitude ranging from 4 to 12 µA (0.1 ms, at least 10 repetitions each) was delivered every 10 s to evoke IPSCs.

Data were acquired using an Axopatch 200B amplifier controlled by pClamp software (v10.7, Molecular Devices), filtered at 2 kHz and sampled at 10 kHz (Digidata 1440A, Molecular

Device). Series resistance (mean±SEM = 22.8±2.00, range 11–29 MΩ) was monitored at regular intervals throughout the recording and only those recordings with series resistance variations of ≤20% were included in the analysis. Data are reported without corrections for liquid junction potentials. Evoked IPSC data were analysed using Clampfit 10.7 (Molecular Devices). The analysed data had passed normality tests and two-way ANOVA and Sidak's multiple comparisons tests were performed using Prism 8 (GraphPad).

Primary neuronal cultures, transfection and immunocytochemistry

Cortical culture on coverslips were prepared from rat (Envigo) embryos at E17. Plasmid transfections were done at 13 days *in vitro* (DIV 13) with 1 µg of total plasmid DNA per coverslip. The plasmid(s) were mixed with 2 µl lipofectamine 2000 (Thermo Fischer Scientific) and 1 µl (1:10 diluted) magnetofection beads (CombiMag, OZ Bioscience). The plasmid-lipofectamine-magnetofection mix were incubated at room temperature for 15 min before adding to neurons. The neuron dishes were placed on top of magnetic plates during the 45 min transfection in the 37°C incubator. The coverslips were transferred to 1 ml conditioned media and returned to the incubator. The plasmids used in the groups are the following: pEGFPC2-gephyrin P1, pEGFPC2-gephyrin K148R, pEGFPC2-gephyrin DN, pEGFPC2-gephyrin S303A/S305A. After one-week of plasmid expression (DIV13+7), the coverslips were rinsed in ice cold PBS, incubated with primary antibody mix containing 10% normal goat serum, GABRA1 (rabbit) and GABRA2 (guinea pig) antibodies was added to the coverslips and incubated for 90 min inside a humidified chamber at 37°C incubator. The coverslips were rinsed in PBS at room temperature (RT), and fixed with 4% PFA for 10 min at RT. After rinsing out the PFA, the coverslips were incubated with corresponding secondary antibodies (see antibody list). Images from ~20 neurons (3 different batches) were analysed for eGFP-gephyrin

clusters colocalization with GABRA1 and GABRA2 containing GABAARs. One-way ANOVA was used to compare between different groups, with post-hoc Tukey test.

Two-Photon quantification and statistical analysis

All individual neurons expressing RCaMP1.07 in a field of view were manually selected as regions of interest (ROIs) on ImageJ and further processed with custom-designed toolbox Cellular and Hemodynamic Image Processing Suite (CHIPS; Barrett et al., 2018) for MATLAB (R2015b, MathWorks). The images for a field of view were first motion-corrected with a 2D convolution engine for x-y drift. The dF/F value from each manually selected ROI was calculated relative to the baseline imaging period before whisker stimulation (the 2.5 seconds from the beginning of each trial). Peaks were identified by the MATLAB findpeaks function following application of a digital band-pass filter (passband frequency of minimum 0.1 Hz and maximum 2 Hz) and a threshold of 5 standard deviations from the baseline. The peak onset time was calculated by the first time point of the smoothed signal trace (2 frames moving average) crossed over the threshold (the mean of the 2.5 seconds baseline plus 1.5 times the standard deviation) after the start of stimulation.

For the analysis, we focused on the 2 second time window indicated in Fig. 2A (1 second of whisker stimulation and 1 second after the stimulation). For the high responders, the cut-off points for amplitude and number of events were defined as ~10% of the neuronal population in WT of the corresponding experiment. The size of the population, amplitude, duration and number of events of the high responders were analysed separately.

Statistical analysis was performed using R (version 3.5.3) with the multcomp package for linear-mixed effect model. We set the following as fixed effects which were tested individually or for their interactions: stimulation condition (with or without whisker stimulation), genotype (for *Gabra1* KO and *Gabra2* KO experiments), Cre (for *Gabra1*$^{flox/flox}$

and *Gabra2*$^{flox/flox}$ experiment, with or without Cre expression), treatment with TAM (for the gephyrin mutant experiment, before or after tamoxifen injections), mutants (for gephyrin the mutant experiment, to compare between different mutants). Individual animal and ROIs were set as random effects. The data were presented with means (un-corrected) and standard error of the means (SEM). The p values reported for different comparisons were obtained by using a Tukey post-hoc test.

Antibody table:

Target	**Distributor/Produce from**	**Description & Ref. no.**	**Dilution**	**Marker of**
GFP	Aves Labs	Chicken, GFP-1020	1:5000	IHC
CaMKIIa	Thermo Fisher Scientific	Mouse, 13-7300	1:1000	IHC
GABRA1	Home-made	Guinea pig	1:10000	IHC
GABRA1	Home-made	Rabbit	1:10000, 1:600	ICC, WB
GABRA2	Home-made	Guinea pig	1:2000	IHC
GABRA2	OriGene	Rabbit, TA327182	1:1000	WB
ACTIN	Millipore	Mouse, MAB1501	1:10000	WB
GEPHYRIN	Synaptic Systems	Mouse	1:1000	WB

Results

$GABA_AR$ subtypes adapt their expression to altered sensory inputs

To determine whether GABAergic synapses are involved in activity-dependent plasticity in the barrel cortex, we assessed whether $GABA_AR$ cell surface expression was altered in response to sensory stimulation or sensory deprivation. We injected an AAV8- CaMKIIα-tdTomato into the lateral ventricles of pups on post-natal day 0 (P0) to achieve wide-scale tdTomato expression in excitatory neurons, including cortical pyramidal cells (Kim et al. 2013). At P60,

we either stimulated the vibrissae bilaterally for one minute every day or trimmed all the whiskers daily for one week (Fig. 1A). The mice were then sacrificed and tdTomato-positive L2/3 pyramidal neurons in the barrel cortex were analyzed for expression of $GABA_AR$ subtypes using immunohistochemistry for α1 or α2 subunit containing-$GABA_ARs$, as α1- or α2-$GABA_AR$ subtypes represent the most abundant synaptic $GABA_ARs$ in the superficial cortical layers (Fritschy and Mohler 1995) (Fig. 1B, C). Cluster analysis with an Image-J plugin (see methods) was performed to identify α1- or α2 subunit staining within the somata, where synapses are predominantly inhibitory, and determined the size and density of α1- or α2-$GABA_AR$ clusters (Fig. 1D-G). The α1-$GABA_AR$ cluster density was reduced after 1-week of whisker stimulation or whisker trimming ($F_{(2, 11)}$=37.18, P<0.0001; Fig. 1D). In contrast, α1-$GABA_AR$ cluster size was increased after 1-week whisker stimulation but did not change after whisker trimming ($F_{(2,10)}$=4.6, P=0.036; Fig. 1E). The α2-$GABA_AR$ cluster density was not changed after either stimulation or trimming ($F_{(2,10)}$=2.27, P=0.153; Fig. 1F), but their cluster size increased in the whisker stimulation group ($F_{(2,10)}$=6.45, P=0.016; Fig. 1G). Together, altered sensory inputs to the barrel cortex led to a dramatic reduction in the number of somatic α1-$GABA_AR$ clusters, while the α1- and α2 subunit containing-$GABA_ARs$ accumulate at inhibitory postsynaptic sites after a week of whisker stimulation. These results indicate that $GABA_AR$ subtypes adapt differently to changes in sensory input, suggesting differential roles for $GABA_AR$ receptor subtypes during sensory processing.

α1-GABA$_A$Rs contribute to sparse pyramidal neuron activity during sensory encoding

The altered expression of $GABA_AR$ subtypes can potentially lead to changes in neuronal activities, affecting the local microcircuit. To evaluate the functional role of α1-$GABA_ARs$ in sensory processing, we made use of the *Gabra1* global gene deletion mouse line (*Gabra1* KO) (Vicini et al. 2001). The activity of the L2/3 pyramidal neurons in the barrel cortex were

435 assessed by using AAV6-CaMKIIα-RCaMP1.07, a red-shifted genetically encoded Ca^{2+}
436 indicator (Ohkura et al. 2012), and *in vivo* 2-photon Ca^{2+} imaging (Fig. 2A). Each neuronal
437 population was imaged three-four times on different days under light anesthesia (1.2%
438 isoflurane). The spontaneous and single whisker stimulation-induced Ca^{2+} transients were
439 imaged and analyzed. In the trials with whisker stimulation, we used a 1-second 90 Hz single-
440 whisker stimulation protocol with a piezo-based stimulator (Mayrhofer et al. 2015; Stobart et
441 al. 2018), and it started 2.5 seconds (baseline) after the trial initiation (Fig. 2A). In order to
442 capture the immediate stimulus-induced Ca^{2+} transients, our analysis was restricted to the time
443 during and after 1 second of whisker stimulation (Figure 2A; right panel). Changes in neuronal
444 activity were assessed by analyzing Ca^{2+} transients for parameters such as amplitude, duration
445 at half-maximum of amplitude, and the number of events per imaging session (40 trials each
446 for spontaneous or whisker stimulation-induced conditions).

447 The single-whisker stimulation induced clear Ca^{2+} responses, while the spontaneous
448 Ca^{2+} transients in the same time window demonstrated no change between WT and *Gabra1*
449 KO mice (Fig. 2B; Suppl. Fig. 1B-B''). However, in *Gabra1* KO animals, L2/3 pyramidal
450 neurons exhibited a higher amplitude of Ca^{2+} transients after whisker stimulation (Fig. 2C).
451 Analysis for the duration and the number of events per neuron (over 40 trials) did not show
452 differences in average values between WT and *Gabra1* KO (Fig. 2C'-C''). Also, the time of
453 onset and decay time of Ca^{2+} events were similar in WT and *Gabra1* KO (Suppl. Fig. 1C-C').

454 Pyramidal neuron activity *in vivo* indicates that roughly 10% of the population in the
455 L2/3 barrel cortex encodes sensory stimulation with robust, high amplitude Ca^{2+} events due to
456 sparse firing (Crochet et al. 2011), even though the Ca^{2+} response magnitude is broadly
457 distributed across the population (Fig. 2C). Based on this knowledge, and to understand how
458 *Gabra1* gene depletion impacts the population distribution of pyramidal neuron activity, we
459 defined a cut-off for high-responding cells as the 90^{th} percentile amplitude value from the WT

neurons and only considered L2/3 pyramidal neurons in the WT and KO groups that had amplitudes greater than or equal to this value (Margolis et al. 2012). In WT mice, these high responders were 11% of the total population, while high responders with amplitudes over the same cut-off mark were 36% of the *Gabra1* KO principal cells (Fig. 2D). This likely accounted for the higher signal amplitudes observed in the *Gabra1* KO population (Fig. 2C). When we compared the Ca^{2+} transient amplitude, duration and number of events within this subset of high-responding neurons, we did not find any difference between the two genotypes, apart from a reduction in the duration of spontaneous Ca^{2+} transients in *Gabra1* KO mice (Fig. 2E-E''). Our results show that α1-$GABA_A$Rs control pyramidal neuron excitability after whisker stimulation and sparseness within the population.

The thalamus plays a central role in relaying the vast majority of sensory information to the cortex. The α1-$GABA_A$Rs expressed within the thalamus have been shown to gate thalamic output to the visual cortex and promote the onset of the critical period of ocular dominance plasticity (Sommeijer et al. 2017). Within the barrel cortex, thalamic afferents innervate mainly L4, with lesser innervations onto L1 and L5 (El-Boustani et al. 2020). To minimize the functional influence originating from the thalamus, we blocked action potentials using tetrodotoxin (TTX) and measured miniature inhibitory postsynaptic currents (mIPSCs) in barrel cortex L2/3 pyramidal neurons of WT and *Gabra1* KO mice. Our electrophysiological recordings showed a significant reduction in the amplitude of GABAergic postsynaptic currents with no changes in the frequency of the events in *Gabra1* KO L2/3 pyramidal neurons (Fig. 2F-H). The *Gabra1* KO L2/3 neurons had faster rise times and slower decay kinetics (Fig.2 I-J). To understand compensatory changes with another $GABA_A$R subunit, we used morphology analysis and stained for VGAT, gephyrin, and α2-$GABA_A$R subtype in WT and *Gabra1* KO mice cortex (Suppl. Fig. 1D). The cluster analysis showed no changes in VGAT and gephyrin density between WT and *Gabra1* KO, but a significant increase in α2-$GABA_A$R

density in *Gabra1* KO tissue (Suppl. Fig. 1E-E''''). However, the increase in α2-$GABA_A$Rs did not fully compensate for the reduced inhibition by the loss α1-$GABA_A$Rs. Together, these results emphasize the essential role of α1-$GABA_A$Rs for modulating microcircuit activity in response to sensory input in the mouse barrel cortex.

α2-$GABA_A$Rs regulate the reliability of L2/3 pyramidal cells responding to sensory inputs

Next, we evaluated the role of α2-$GABA_A$Rs using a *Gabra2* gene global deletion mouse line (*Gabra2* KO) (Panzanelli et al. 2011; Koester et al. 2013). Similar to the approach described above for *Gabra1* KO, spontaneous or stimulation-induced pyramidal neuron Ca^{2+} transients were measured (Fig. 3A-A'). Analysis of spontaneous Ca^{2+} transients showed no genotype effect on amplitude (Suppl. Fig. 2A, B). We observed a wider distribution of signal amplitudes in *Gabra2* KO upon whisker stimulation. Although the mean amplitudes between WT and *Gabra2* KO were not different, the majority of *Gabra2* KO cells had lower than average Ca^{2+} amplitude, and a small sub-group had higher than average amplitude responses (Fig. 3B as an example). The durations of spontaneous Ca^{2+} transients were similar between WT and *Gabra2* KO (Suppl. Fig. 2B', B''); however, after whisker stimulation, Ca^{2+} transients tended to have a shorter duration ($p=0.13$; Fig. 3B'). When considering the number of Ca^{2+} events per neuron across all trials, the frequency of spontaneous activity was similar between *Gabra2* KO and WT cells (Suppl. Fig. 2B''). Still, whisker stimulation evoked fewer (~50%) Ca^{2+} transients in *Gabra2* KO, indicating reduced reliability of pyramidal neurons to repetitively encode whisker stimulation (Fig. 3B''). In addition, we observed slower onset and longer decay time of Ca^{2+} transients after whisker stimulation in *Gabra2* KO compared to WT (Suppl. Fig. 2C-C').

To evaluate whether *Gabra2* gene deletion also influences the population distribution of highly responsive pyramidal neurons, we set a cut-off according to the amplitudes of the WT group, as described in the previous section. Using this amplitude value, we found that 21%

of pyramidal neurons were high responders in *Gabra2* KO mice (Fig. 3C). Within this subset of high responding cells, the amplitude of both spontaneous and whisker stimulation-induced Ca^{2+} transients in *Gabra2* KO was higher than in WT high-responders (Fig. 3D). At the same time, there was no difference in the duration of spontaneous or whisker stimulation-induced events (Fig. 3D'). Although the number of events per neuron occurring under spontaneous activity was not different between high amplitude pyramidal neurons of each genotype, the number of events evoked by whisker stimulation was reduced in *Gabra2* KO (Fig. 3D''). Our data suggest that α2-$GABA_A$Rs influence the success rate of whisker stimulation-triggered neuronal responses and partially contribute to the sparseness of the high-responding pyramidal neurons by increasing the neuronal activity in a small set of the neuronal population.

To evaluate how α2-$GABA_A$Rs contribute to the Ca^{2+} transients of L2/3 pyramidal neurons, we blocked action potentials using tetrodotoxin (TTX) and measured miniature inhibitory postsynaptic currents (mIPSCs) in barrel cortex L2/3 pyramidal neurons of WT and *Gabra2* KO mice. Our electrophysiological recordings showed increased mIPSC amplitude in *Gabra2* KO (Fig. 3E, F), and the inter-event intervals were reduced (Fig. 3G). The rise time for receptors did not change in the *Gabra2* KO, while the decay kinetics was reduced (Fig. 3H, I). The observed changes in electrophysiological properties within *Gabra1* KO and *Gabra2* KO suggest that compensatory changes at synaptic sites are different in the absence of α1 or α2 subunit-containing $GABA_A$Rs. We stained for VGAT, gephyrin, and α1-$GABA_A$R subtype in WT and *Gabra2* KO mice cortex (Suppl. Fig. 2D). The cluster analysis showed no changes in VGAT, gephyrin, or α2-$GABA_A$R density between WT and *Gabra2* KO (Suppl. Fig. 2E-E'''').

To understand compensatory changes of $GABA_A$R subunits at the protein level, we used Western blot analysis to assess barrel cortex tissue and measured expression changes in α2 and α3 subunits in *Gabra1* KO and α1 and α3 subunits in *Gabra2* KO (Suppl. Fig. 3). As

shown previously (Kralic et al. 2006), expression of the α3 subunit was increased in *Gabra1* KO with no change in α2 subunit levels (Suppl. Fig. 3A, A'). In *Gabra2* KO tissue, we also found an increase in the α3 subunit expression but no change in α1 subunit expression (Suppl. Fig. 3B, B'). The increased expression of α3, however, is unlikely to account for observed effects on Ca^{2+} transients in the *Gabra1* and *Gabra2* KOs.

Cell-autonomous effects of $GABA_AR$ subtypes within barrel cortex microcircuits

While our results strongly suggest that $GABA_AR$ subtypes are important for modulating microcircuit activity and contribute to function differentially, the compensation from other $GABA_AR$ subtypes in the global KO models appears to be prominent. Hence, we moved to the $Gabra1^{flox/flox}$ or $Gabra2^{flox/flox}$ mice to conditionally ablate the *Gabra1* or *Gabra2* gene from adult L2/3 pyramidal neurons using cell-type-specific Cre expression. We injected AAV6-CaMKIIα-RCaMP1.07 or co-injected AAV6-CaMKIIα-eGFP-Cre and AAV6-CaMKIIα-RCaMP1.07 into the barrel cortex and compared Ca^{2+} transients between RCaMP only cells (control) and Cre-positive RCaMP cells (Fig. 4A). Post-mortem validation of the deletions of GABRA1 and GABRA2 in $Gabra1^{flox/flox}$ and $Gabra2^{flox/flox}$ mice was done by immunohistochemistry (Suppl. Fig. 4A-B)

Next, we quantified changes in Ca^{2+} transients in $Gabra1^{flox/flox}$ mice (Fig. 4B-B''; Suppl. Fig. 4C-E). The RCaMP control pyramidal neurons showed an apparent increase in Ca^{2+} amplitude to whisker stimulation. Surprisingly, the Cre-positive RCaMP cells did not show an increase in Ca^{2+} amplitude upon whisker stimulation (Fig. 4B). Similarly, the Cre-positive neurons showed no change in duration and number of events. Interestingly, the number of events was largely reduced in the cells with Cre-expression (Fig.4B''; Spontaneous: control vs. cre-positive, p=0.1616; Whisker stimulation: control vs. cre-positive, ***p<0.001). To understand whether the local microcircuit is compromised in the absence of α1-$GABA_ARs$, we

560 analysed the Cre-negative RCaMP neurons next to the Cre-positive RCaMP neurons. Our
561 analysis of Ca^{2+} transients in the Cre-negative cells showed similar results as Cre-expressing
562 neurons upon whisker stimulation (Suppl. Fig. 4E). This indicates a subpopulation of neurons
563 lacking α1-$GABA_A$Rs can influence the local microcircuit activity more strongly than one had
564 anticipated. Together, our data identify that in the absence of α1-$GABA_A$Rs, L2/3 pyramidal
565 neurons exhibit reduced excitability, which contrasts with our global *Gabra1* KO data.

566 We used the same approach to assess Ca^{2+} transient changes in *Gabra2*$^{flox/flox}$ mice (Fig.
567 4C-C''; Suppl. Fig. 4F). The effect of removing α2-$GABA_A$R could be assessed by comparing
568 RCaMP control with Cre-positive RCaMP cells. Upon whisker stimulation, Ca^{2+} amplitude
569 and the number of events significantly increased in all groups (Fig. 4C, C''). However, the
570 baseline amplitude in Cre-positive RCaMP areas was higher (control vs. Cre-positive,
571 *p=0.012). Similar to *Gabra1*$^{flox/flox}$ animals, we analyzed Cre-negative RCaMP cells
572 neighboring the Cre-positive cells and uncovered that they showed a tendency towards the
573 extended duration of Ca^{2+} transients (Suppl. Fig. 4F middle panel). In contrast to the global
574 *Gabra2* KO results, conditional deletion of *Gabra2* in L2/3 pyramidal neurons reduces
575 inhibition. Furthermore, showing an increase in Ca^{2+} transient amplitude and number of events
576 in Cre-negative RCaMP cells upon whisker stimulation suggests that removing α2-$GABA_A$Rs
577 also functionally contributes to reciprocal connections within L2/3 pyramidal cells and their
578 role in maintaining local circuit dynamics.

579 We further examined the subpopulation of high-responding neurons in spontaneous and
580 whisker stimulation-induced conditions in *Gabra1*$^{flox/flox}$ or *Gabra2*$^{flox/flox}$ mice (Fig. 4D-D'). In
581 *Gabra1*$^{flox/flox}$ mice, 50% of Cre-positive group exhibited high-responding population in
582 spontaneous activity. However, only 21% of high-responding cells had increased Ca^{2+}
583 transients after whisker stimulation. In *Gabra2*$^{flox/flox}$ mice, 80% of Cre-positive neurons
584 exhibited higher spontaneous activity compared to 10% in the control neurons. This

585 representation of high-responsive cells remained at 65% after whisker stimulation. In
586 summary, our results demonstrate that α1- and α2-$GABA_A$Rs in L2/3 pyramidal neurons have
587 distinctive roles in controlling neuronal excitability at the individual level and local
588 microcircuit level. While removal of α1-$GABA_A$R subtypes dampens excitability of the L2/3
589 circuit, removal of α2-$GABA_A$R subtypes facilitates excitability of the circuit.
590
591 ***Gephyrin scaffold dynamics influence GABAergic neurotransmission in vivo***
592 $GABA_A$Rs synapse recruitment via lateral mobility on the plasma membrane, receptor
593 insertion at extrasynaptic sites, internalization, and degradation of synaptic receptors are all
594 dynamically facilitated by gephyrin and various PTMs on it (Tyagarajan and Fritschy 2014).
595 Hence, it is logical that we also ascertain the *in vivo* relevance of this scaffolding protein for
596 α1- or α2-$GABA_A$R function within the barrel cortex. Of the various PTMs reported for
597 gephyrin, phosphorylation at Ser 303 and Ser 305 sites is known to be activity-dependent
598 (Flores et al., 2015). It has been reported that phosphorylation of S303 and S305 residues by
599 protein kinase A (PKA) and calcium calmodulin kinase II α (CaMKIIα) respectively facilitates
600 NMDA receptor-dependent $GABA_A$R recruitment at inhibitory terminals (Flores et al. 2015).
601 Similarly, SUMOylation at Lys 148 is known to stabilize gephyrin scaffold and GABAergic
602 synapses (Ghosh et al. 2016). Therefore, we selected phosphorylation-null gephyrin mutants
603 S303A/S305A (SSA) to block the activity-dependent recruitment of $GABA_A$Rs to postsynaptic
604 sites. Alternatively, we selected the K148R gephyrin mutant to stabilize $GABA_A$Rs at synaptic
605 sites. A SUMO1 conjugation-defective mutant (K148R) has been reported to stabilize sub-
606 membrane gephyrin clusters at inhibitory postsynaptic sites (Ghosh et al. 2016). In addition,
607 we used the dominant negative mutant (DN) lacking the last 12 amino acids to disrupt gephyrin
608 scaffolding and GABAergic neurotransmission *in vitro* (Ghosh et al. 2016) (Fig. 5A).

609 The functional impact of a static gephyrin scaffold or the absence of a gephyrin scaffold
610 at GABAergic postsynaptic sites in L2/3 pyramidal neurons was characterized. For this, we
611 injected AAV6-hSyn1-flex-eGFP-gephyrin variants, AAV6-CaMKIIα-ERT2-Cre and AAV6-
612 CaMKIIα-RCaMP1.07 to co-express eGFP-gephyrin variants and RCaMP1.07 in L2/3
613 principal cells. This combination of viruses was also used to evaluate activity changes in
614 pyramidal neurons with *in vivo* 2-photon Ca^{2+} imaging (see the next section). After four weeks
615 of virus co-expression, we injected tamoxifen intraperitoneally (i.p) for four consecutive days
616 to activate Cre recombinase and allowed the expression of gephyrin mutant variants (Fig. 5B).
617 We then waited for a least seven days and then recorded miniature inhibitory postsynaptic
618 currents (mIPSC) from L2/3 pyramidal neurons overexpressing the respective gephyrin
619 transgenes in acute slices of barrel cortex, in the presence of tetrodotoxin (TTX), CNQX and
620 AP-5 (Fig. 5C). Neurons expressing the transgene gephyrin-DN demonstrated reduced mIPSC
621 amplitude (14.6 ± 1.6 pA) with respect to GFP controls (28.8 ± 2.0 pA; $P<0.0001$). The mIPSC
622 inter-event interval (IEI) increased in gephyrin-DN neurons, indicating the frequency was
623 reduced (inter-event intervals: 1451 ± 463.2 ms; GFP=659.9 ± 78.3 ms; P=0.038; Fig. 5D).
624 The distribution of IEI for DN is wider, so we further examine its lognormality by performing
625 D'Agostino-Pearson test, in addition to QQ-plot (Suppl. Fig. 5). The results suggest that the
626 distribution of IEI for DN follows the normal distribution. It is known that gephyrin-DN
627 destabilizes synaptic $GABA_AR$s *in vitro*, and perhaps a similar mechanism reduces the
628 availability of synaptic $GABA_AR$ in gephyrin-DN-expressing neurons. The neurons expressing
629 gephyrin-SSA mutation demonstrated mIPSCs of increased amplitude (37.8 ± 2.7 pA;
630 P=0.026; Fig. 5D), likely as a result of increased $GABA_AR$ retention at synaptic sites (Battaglia
631 et al. 2018). Finally, the expression of gephyrin transgene with the K148R mutation had no
632 effect on mIPSC amplitude compared to controls (28.8 ± 2.0 pA vs. 25.6 ± 1.8 pA; P=0.641).
633 The inter-event interval (IEI) was not different between the gephyrin mutants (eGFP: 659.9 ±

634 78.3 ms; gephyrin-K148R: 408.0 ± 56.3 ms; gephyrin-SSA: 401 ± 73.7 ms), suggesting that
635 there were no major changes in spontaneous neurotransmitter release or in the number of
636 GABAergic inhibitory synapses (Fig. 5D).

637 Overall, our results suggest that the majority of the GABAergic postsynaptic sites
638 containing gephyrin are influenced by cellular signaling events that directly impact PTMs on
639 gephyrin. Importantly, different gephyrin mutants influence GABAergic neurotransmission in
640 a mutually exclusive manner.

641

642 ***Gephyrin mutant expression influences whisker stimulation-induced Ca^{2+} transients***

643 As gephyrin scaffold can impact GABAergic neurotransmission in an opposite manner, we
644 measured changes in Ca^{2+} transients in pyramidal neurons before and after gephyrin-mutant
645 expression. Gephyrin-mutant expression was controlled by tamoxifen-inducible Cre
646 expression. We confirmed that around 40% of the pyramidal cells co-expressed all three viral
647 vectors: AAV6-hSyn1-flex-eGFP-gephyrin variants, AAV6-CaMKIIα-ERT2-Cre and AAV6-
648 CaMKIIα-RCaMP1.07 (Suppl. Fig. 6). As an additional control, we expressed RCaMP1.07 in
649 a neighboring barrel area (Area 1) (Fig. 6A). We examined all RCaMP-expressing neurons and
650 compared changes in Ca^{2+} transients before and after eGFP-gephyrin expression. Examples of
651 average Ca^{2+} transient changes in response to whisker stimulation both before and after
652 gephyrin-mutant expression are shown (Fig. 6B). The activity of individual neurons was
653 normalized to activity before tamoxifen (TAM) injection [(After-Before)/Before] to identify
654 relative changes.

655 The gephyrin-mutant expression did not influence spontaneous Ca^{2+} transient
656 amplitude and number of events compared to the control (area1) (Suppl. Fig. 7A, A''). However, gephyrin-K148R mutant expression reduced spontaneous Ca^{2+} duration (Suppl. Fig.
657 7A'). Upon whisker stimulation, the gephyrin-K148R mutant caused no change in any of the
658

parameters (Fig. 6C-C"). The gephyrin-SSA mutant expression decreased the amplitude of evoked events, while the gephyrin-DN mutant increased the amplitude of Ca^{2+} transients (P=0.373; Fig. 6C). The duration of Ca^{2+} transients was mostly unaffected by the expression of either of the gephyrin mutants (Fig. 6C'). Expression of the gephyrin-SSA and gephyrin-DN mutants reduced and increased the number of events, respectively (Fig. 6C''). Furthermore, onset and decay times were similar before and after the expression of gephyrin variants (Fig. 6D). The influence of gephyrin mutant variant expression on Ca^{2+} transient changes was consistent with their impact on inhibitory neurotransmission changes observed using the patch clamp technique (Fig. 5).

We previously identified high responding cells in both conditional and global KO of α1- and α2-$GABA_AR$ subunits (Figs. 2-4). We used a similar strategy to group neurons based on their Ca^{2+} transients' amplitude or the number of events within our gephyrin mutant populations (Suppl. Fig. 7B-C). As expected, in control neurons (Area 1), the amplitude and number of events within the populations remained comparable before and after tamoxifen injection. Similarly, gephyrin-K148R mutant expression did not impact the population distribution based on amplitude changes (Suppl. Fig. 7B). However, expression of gephyrin-SSA and gephyrin-DN mutants had the most impact on amplitude changes within the given population of neurons. Specifically, gephyrin-SSA mutant expression led to a smaller population of neurons responding with high amplitude. In contrast, gephyrin-DN mutant expression increased the population of high amplitude neurons by 20% (Suppl. Fig. 7B). The number of Ca^{2+} transient event distributions was not affected upon gephyrin-K148R or gephyrin-SSA expression but was vastly increased in gephyrin-DN mutant expressing L2/3 pyramidal neurons (Suppl. Fig. 7C). Specifically, the cell population exhibiting 21-30 events increased from 29% to 49% and 31-40 events increased from 4% to 10%. The effects of

683 gephyrin mutants on mIPSC amplitudes and frequencies are consistent with the Ca^{2+} transients
684 measured in pyramidal neurons expressing individual gephyrin mutants.

685 To confirm gephyrin mutation has direct functional impact on L2/3 pyramidal neuron
686 excitability, we recorded stimulation-evoked IPSCs from gephyrin-DN expressing neurons.
687 For this, we infected AAV8-mCaMKIIα-mCherry-2A_iCre and AAV6-hSyn-flex-eGFP or
688 AAV6-hSyn-flex-eGFP-gephyrin-DN were stereotactically injected into L2/3 of the barrel
689 cortex. In both conditions, the co-expression of mCherry and eGFP allowed the identification
690 of co-infected pyramidal neurons. We found that the input/output curve of the eIPSC amplitude
691 at different stimulus intensities for gephyrin-DN mutant was significantly reduced as compared
692 to eGFP control specifically when the stimulus intensity was high. (Suppl. Fig. 5C, D). A two-
693 way ANOVA of eIPSCs revealed that the interaction between the effects of the gephyrin virus
694 and stimulus intensity was statistically significant ($F(8, 56) = 3.745$, $P=0.0014$). The results
695 suggest that the manipulation of gephyrin scaffolds by gephyrin-DN overexpression leads to
696 an activity-dependent reduction of inhibition on L2/3 pyramidal neurons in the barrel cortex.
697 Overall, our data identify the gephyrin scaffold as an essential component for response
698 reliability to sensory inputs, and modulations of the gephyrin scaffold in a subset of pyramidal
699 neurons were sufficient to fine-tune the population response to whisker stimulation.
700

701 ***Gephyrin mutants show a preference for $GABA_AR$ subtypes***

702 *In vitro* studies have identified gephyrin scaffold as a signaling hub at GABAergic postsynaptic
703 sites to facilitate activity-dependent synaptic $GABA_AR$ recruitment and removal. However, it
704 remains unclear how specific PTM on gephyrin alters its ability to recruit either α1- or α2-
705 containing $GABA_ARs$. To understand this better, we used cortical primary neuron culture and
706 examined the co-localization of α1 or α2 subunits with eGFP-gephyrin mutants. We
707 transfected primary cortical neurons with either eGFP-gephyrin (WT), eGFP-gephyrin K148R,

eGFP-gephyrin SSA, or eGFP-gephyrin DN at 13 days in vitro (13 DIV). At 20 DIV, the cultures were co-stained for α1 and α2 $GABA_AR$ subunits (Fig. 7). The eGFP-gephyrin or its mutant variants were co-labelled with α1 and α2 $GABA_ARs$, except the DN mutant that showed diffuse signal across soma and dendrites and α1, α2 $GABA_ARs$ were also diffusely labeled in DN expressing neurons. The eGFP-gephyrin and its mutants exhibited phenotypes consistent with earlier reports (Flores et al. 2015; Ghosh et al. 2016). Our cluster analysis to determine the colocalization of eGFP-gephyrin or its mutants with either α1 or α2 $GABA_ARs$ showed differential preference. The colocalization of WT, SSA, and K148R mutant gephyrin with α1 containing $GABA_ARs$ was not significantly different (Fig. 7B). However, SSA mutant exhibited significantly reduced colocalization with α2 containing $GABA_ARs$ (Fig. 7B'). The overall density of α1 $GABA_ARs$ was not altered in neurons expressing either WT or mutant eGFP-gephyrin (Fig. 7C), but the neuron expressing K148R mutant gephyrin had a significantly bigger α1 $GABA_AR$ cluster size (Fig. 7C'). The cluster density and size of α2 $GABA_ARs$ were similar in neurons expressing either eGFP-gephyrin WT, SSA, or K148R (Fig. 7D, D'). Our results highlight the significance of different post-translational modifications on gephyrin for the recruitment of specific $GABA_AR$ subtypes to facilitate cortical circuit function.

Discussion:

Somatosensory information is processed in a selective manner and is encoded sparsely. While it is well established that GABAergic inhibition plays a central role in sparse sensory processing, the contribution of $GABA_AR$ subtypes to the functional specificity of the somatosensory cortex microcircuit is unknown. To fill this knowledge gap, we present data from three groups of cells from floxed *Gabra1* mice or floxed *Gabra2* mice: RCaMP in naïve animals (controls), RCaMP analysis from Cre+ L2/3 pyramidal neurons, and RCaMP analysis from Cre- L2/3 pyramidal neurons (cells neighboring the Cre+ ones). This data set provides

733 the unique opportunity to study the conditional deletion of alpha subunits (Cre +ve cells) vs.
734 control and changes that occur in other nearby pyramidal cells (Cre -ve cells) in the same
735 microcircuit.

736 Our results from these three groups underscore the contribution of α1- and α2-
737 containing receptors for intrinsic pyramidal neuron excitability and the microcircuit function
738 (which involves pyramidal-pyramidal-GABAergic interneuron interconnectivity to form a
739 local circuit). We also report that at the morphological level, neuronal expression of α1- and
740 α2-$GABA_A$Rs are differentially altered after sensory stimulation and deprivation.

741 We link the functional contributions of α1- or α2- $GABA_A$Rs to their main scaffolding
742 protein gephyrin, and its dynamic scaffolding configurations facilitated by PTMs. Specifically,
743 we show that sites S303/S305 phosphorylated in consequence to glutamatergic synapse activity
744 reduces gephyrin colocalization with α2-$GABA_A$Rs. Similarly, expression of gephyrin-SSA
745 mutant *in vivo* had the most impact on amplitude changes within L2/3 neurons after whisker
746 stimulation. Specifically, gephyrin-SSA mutant expression led to a smaller population of
747 neurons responding with a high amplitude of Ca^{2+} transients (Suppl. Fig. 7B). On the other
748 hand, stabilizing gephyrin scaffold using K148R mutation facilitated the recruitment of more
749 α1-$GABA_A$Rs to synapses. *In vivo* expression of gephyrin-K148R mutant had no impact on
750 the population distribution based on amplitude changes (Suppl. Fig. 7B). By linking the
751 gephyrin mutant study with global and cell-specific conditional *Gabra1* or *Gabra2* KO, our
752 results provide the first direct evidence linking gephyrin scaffold dynamics to $GABA_A$R
753 selectivity and L2/3 pyramidal neuron responses upon sensory inputs.
754
755 ***Neuronal network activity defined by $GABA_A$R subtypes***
756 We provide evidence that global ablation of α1-$GABA_A$Rs increases pyramidal cell
757 excitability and dampens L2/3 pyramidal neuron inhibition. On the other hand, L2/3 pyramidal

neuron-specific deletion of *Gabra1* reduces excitability at both single cell and microcircuit levels. Why would the conditional loss of an inhibitory receptor subunit lead to a decrease in neuronal responses (at rest and during sensory stimulation)? In other aspects of our study, we found similar results where neuronal responses and the number of events were reduced in two other cases. First, in *Gabra2* KO mice, there was a decrease in the number of Ca^{2+} events in the whole population and an increase in the mIPSC amplitude measured by electrophysiology (Fig. 3). Furthermore, there was an increase in GABRA3 expression (Supp. Fig. 3), indicative of an upregulation of other inhibitory subunits, which may account for the observed changes in Ca^{2+} and mIPSCs. Second, expression of gephyrin mutant SSA also decreased the number of Ca^{2+} events (Fig. 6C") and increased the mIPSC amplitude (Fig. 5), which may occur as a result of increased $GABA_AR$ retention at synaptic sites (Battaglia et al. 2018). In both of these cases, the results suggest an increased inhibitory tone on pyramidal cells, possibly due to the upregulation of other subunits. In the case of *Gabra1* floxed mice, the precise mechanism of this change remains to be investigated in future studies by electrophysiology and histology for *Gabra* subunit clusters, but it suggests that there is an imbalance in the inhibitory activity that occurs in the whole circuit (both cells with the *Gabra1* deletion and their neighbors). Other *Gabra* subunits (such as *Gabra3*) could be elevated as compensation.

The global ablation of α2-$GABA_ARs$ reduces pyramidal cell excitability, microcircuit activity and increases inhibition in L2/3 pyramidal neurons. The L2/3 pyramidal neuron-specific deletion of *Gabra2* increases pyramidal cell excitability and microcircuit activity. In addition, α2-$GABA_ARs$ contribute to the reliability of neuronal responses to whisker stimulation. When *Gabra2* subunits are conditionally deleted (Cre + cells), there is a drastic increase in Ca^{2+} activity. Both Ca^{2+} amplitude and the duration of events increase during spontaneous activity and whisker stimulation (Fig. 4C, C'). This suggests that inhibition of pyramidal cells is lost, leading to increased firing that translates to larger Ca^{2+} events.

783 Interestingly, this elevation in neuronal activity also impacts nearby neighboring pyramidal
784 cells that do not have *Gabra2* deletion (Cre- cells). This suggests that the loss of *Gabra2* was
785 probably not functionally compensated by other alpha subunits. Further, this emphasizes the
786 reciprocal connections within L2/3 circuits and their role in maintaining circuit dynamics.
787 Future studies will help to disentangle the mechanisms behind these changes in *Gabra2* floxed
788 mice.

789 Barrel cortex plasticity is a multifaceted process involving multiple synaptic and
790 cellular mechanisms. Our data posits that $GABA_AR$ subtypes are well placed to regulate
791 various aspects of synaptic plasticity mechanisms to recruit silent neurons into the active
792 population. Whether any specificity exists between a $GABA_AR$ subtype and a subgroup of
793 interneurons is highly debatable. It has been proposed that specific $GABA_AR$ subtypes are
794 allocated to distinct interneuron terminals, thereby defining a functional circuit. For example,
795 it has been suggested that α1-$GABA_ARs$ are localized at PV+ basket cell terminals, while α2-
796 $GABA_ARs$ are localized at CCK+ cell terminals (Nyíri, Freund, and Somogyi 2001; Freund
797 2003). However, it was subsequently reported that α1-and α2-$GABA_AR$ subtypes could be
798 localized at both CCK+ and PV+ terminals (Kerti-Szigeti and Nusser 2016). While the α-
799 subunit has been long thought to be an essential factor determining the allocation of $GABA_ARs$
800 to different postsynaptic sites, it was recently reported that $GABA_ARs$ containing β3 subunits
801 are allocated specifically to PV+ terminals but not SOM+ connections (Nguyen and Nicoll
802 2018). Hence, there are multiple molecular determinants underlying $GABA_AR$ synapse
803 allocation, and these factors add an additional layer of complexity to understanding circuit
804 activity.

805 In hippocampal pyramidal neurons, α2-$GABA_ARs$ are preferentially expressed at the
806 axon-initial segment (AIS) when compared with α1- or α3-containing $GABA_ARs$ (Nusser et
807 al. 1996; Muir and Kittler 2014). In the somatosensory cortex, this compartmentalized

distribution of $GABA_AR$ subunits is less clear, as α1, α2, and α3 subunits exhibit a similar distribution ratio between the AIS compartment and non-AIS compartment (Gao and Heldt 2016). Subcellular localization differences between $GABA_ARs$ are also influenced by lateral surface mobility in response to network activity changes, thereby contributing to synaptic scaling mechanisms (Bannai et al. 2009). Specifically, at AIS, α2-$GABA_ARs$ show lower mobility compared to α1-$GABA_ARs$ (Muir and Kittler 2014). Therefore, the abundance of α2-$GABA_ARs$ at synapses might facilitate membrane depolarization to a greater extent than other $GABA_AR$ subtypes. It has been reported that stimulating GABAergic axo-axonic cells can elicit action potentials in the postsynaptic pyramidal neurons from L2/3 somatosensory cortex (Szabadics et al. 2006). Hence, α1- and α2-$GABA_ARs$ at AIS are well positioned to facilitate pyramidal neuron excitability.

$GABA_AR$ subtypes facilitate sparse encoding in L2/3 pyramidal cells

Sparse coding within pyramidal neurons is determined by changes in excitation-inhibition balance (Andermann and Moore 2006). The L2/3 pyramidal neurons have more hyperpolarized resting potentials; therefore, they require more excitatory input and/or reduced GABAergic input to overcome the action potential threshold (Lefort et al. 2009). Our data demonstrate that $GABA_AR$ subtypes within L2/3 pyramidal neurons are well placed to contribute to circuit-specific sub-threshold excitation and sparse action potential firing. Using $Gabra1^{flox/flox}$ and $Gabra2^{flox/flox}$ mice, we demonstrate that a greater proportion of pyramidal neurons become high-responders upon whisker stimulation. In our experiments, we present data from three groups of cells from $Gabra1^{flox/flox}$ and $Gabra2^{flox/flox}$ mice: RCaMP in naïve animals (controls), RCaMP analysis from Cre-positive L2/3 pyramidal neurons, and RCaMP analysis from Cre-negative pyramidal neurons (neighboring Cre-positive cells; Suppl. Fig.4 E, F). This data set allowed us to study the effects of conditional deletion of α1 or α2 subunits of $GABA_ARs$ (Cre+

cells) vs control, but also changes that occur in other nearby pyramidal cells (Cre- cells) in the same microcircuit. Our results from these three groups highlight the contribution of α1 and α2 subunit-containing $GABA_A$Rs towards intrinsic pyramidal neuron excitability and also microcircuit function (which involves pyramidal-pyramidal-GABAergic interneuron interconnectivity to form a local circuit).

In our experiments, we obtained up to 40% co-expression of eGFP-gephyrin mutants with RCaMP and Cre within the L2/3 pyramidal neurons. In spite of this small-scale co-infectivity ratio, we successfully perturbed microcircuit function upon gephyrin-mutant expression in the barrel cortex. Importantly, we showed a role for cellular signaling and gephyrin scaffold PTMs in modulating the size of responding neuronal population to single-whisker stimulation. Disruption of the gephyrin scaffold through the expression of the gephyrin-DN-mutant led to an expansion in neuronal populations with higher amplitude in Ca^{2+} transients. On the other hand, expression of the gephyrin-SSA mutant led to a decrease in the number of high responder cells (Suppl. Fig. 7). Although a population of gephyrin-dependent and independent $GABA_A$Rs co-exist, the gephyrin-containing inhibitory synapses functionally dominate and facilitate dynamic shifts in Ca^{2+} transient amplitude adjustments (Suppl. Fig. 7B).

$GABA_A$Rs and gephyrin-mediated homeostatic adaptations within L2/3 microcircuit

It is currently hypothesized that both Hebbian and non-Hebbian synaptic plasticity mechanisms might underlie the strengthening and weakening of cellular responses after whisker stimulation and/or trimming (Turrigiano and Nelson 2000; Hofer et al. 2011; Crochet et al. 2011; Margolis et al. 2012). We observed both strengthening and weakening of pyramidal neuron activity, depending on the α1- or α2-$GABA_A$R deletion or gephyrin mutant expression, suggesting that both receptor and its scaffolding protein contribute to homeostatic plasticity mechanisms

858 within cortical L2/3 microcircuit. For example, the ratio of high responders that encoded the
859 whisker stimulus increased in *Gabra1* and *Gabra2* global or conditional KO mice, while the
860 number of Ca^{2+} transients during stimulation decreased (Fig. 2, 3, 4). Furthermore, we found
861 an increase in the mIPSC amplitude in global *Gabra2* KO mice (Fig. 3F). This suggests that
862 the excitation of the pyramidal neuronal network is scaled down in cases of *Gabra2* global KO
863 and *Gabra1* pyramidal neuron-specific KO, even though an inhibitory receptor subtype is lost.
864 These observed changes in pyramidal neuron activity are also reflected upon gephyrin mutant
865 expression *in vivo*, suggesting that homeostatic plasticity mechanisms at GABAergic synapses
866 cannot be completely uncoupled from the receptor and its scaffolding protein.

867 The gephyrin scaffold is known to interact with α1-$GABA_A$Rs and α2-$GABA_A$Rs
868 (Tyagarajan and Fritschy 2014). Independent quantum dot–based single-$GABA_A$R tracking
869 studies have shown that the gephyrin scaffold influences $GABA_A$R surface mobility and
870 synapse retention (Choquet and Triller 2013). Specifically, it was recently shown that gephyrin
871 PTMs, specifically the gephyrin-SSA mutant, increase the synaptic confinement of α2-
872 $GABA_A$Rs in response to 4-Aminopyridine-induced circuit activation (Battaglia et al. 2018).
873 Supporting this finding, our electrophysiology data demonstrated an increase in mIPSC
874 amplitude in gephyrin-SSA expressing neurons (Fig. 5), and *in vivo* imaging data showed that
875 a less excitable population of neurons doubled in size upon gephyrin-SSA expression and
876 whisker stimulation (Suppl. Fig. 7B). Increased synaptic confinement of $GABA_A$Rs in
877 gephyrin-SSA expressing neurons could disrupt dynamic shifts in reducing inhibitory synapses
878 according to excitatory inputs in a neuron. On the other hand, it has been demonstrated that
879 gephyrin-DN expression increased diffusion and exploration of α2-$GABA_A$Rs at both synaptic
880 and extrasynaptic sites (Battaglia et al. 2018). In our electrophysiology studies, we observed
881 increases in mIPSC IEI and reduced amplitude upon gephyrin-DN mutant expression (Fig. 5).
882 *In vivo* imaging data demonstrated that gephyrin-DN mutant expression increases the

883 population of high responders after whisker stimulation by 20% (Suppl. Fig. 7B). Our data
884 implicate a dynamic recruitment model for specific $GABA_AR$ subtypes based on gephyrin
885 PTM. This would mean that specific demand would trigger a signaling cascade to converge
886 onto the gephyrin scaffold. The PTM change on gephyrin in turn would switch affinity towards
887 specific $GABA_AR$ subtype for synapse recruitment.

888 Independent of gephyrin scaffold modulation, a mechanism involving microRNA
889 miR376c was recently reported to specifically regulate dendritic α1 and α2 subunit expression
890 after inhibitory long-term potentiation (iLTP), but not α3, α4, α5 subunit containing-
891 $GABA_ARs$ (Rajgor et al. 2020). This highlights a role for multiple context-dependent
892 $GABA_AR$ modulations at inhibitory synapses.

893 In summary, while it is known that the distribution of activity within cortical neurons
894 is sparse, our data demonstrate that pyramidal neuron excitability is defined by $GABA_A$
895 receptor subtypes and facilitated by gephyrin scaffold dynamics. Our results have characterized
896 the first-time molecular components that are operational at GABAergic postsynaptic terminals
897 to refine and define the sparse sensory encoding process in adult mice.

898

899 **Acknowledgements**

900 We thank J-M. Fritschy for comments on the manuscript and M. Müller for comments on the
901 electrophysiology data. The study was supported by UZH Forschungskredit Can-doc grant to
902 Y-C. Tsai, Olga Mayenfisch Foundation grant, Swiss National Science Foundation grants
903 (31003A_159867 and 310030_192522) and University of Zurich internal funding to S.K.
904 Tyagarajan. Fig. 4 was partially created using BioRender.

905

906 **Author contributions**

907 SKT and YCT conceptualised the study. SKT, YCT and JLS contributed to the design of
908 experiments. YCT performed all 2-photon imaging experiments, JLS aided the data analysis.
909 YCT wrote the first draft of the manuscript. SKT, BW, JLS, KDF and MJPB provided technical
910 knowledge and data analysis support. MH carried out electrophysiological experiments and the
911 analysis. KO, AA conducted surgeries for virus injections. KO, AC, TK helped with evoked
912 response recordings. PP and TC helped with the morphological staining and analysis. All
913 authors contributed to the writing and editing of the manuscript.
914
915 **Competing financial interests**
916 The authors declare no competing financial interests.
917
918 **References**
919 Andermann, Mark L, and Christopher I Moore. 2006. "A Somatotopic Map of Vibrissa
920 Motion Direction within a Barrel Column." *Nature Neuroscience* 9 (4): 543–51.
921 https://doi.org/10.1038/nn1671.
922 Avermann, Michael, Christian Tomm, Celine Mateo, Wulfram Gerstner, and Carl C. H.
923 Petersen. 2012. "Microcircuits of Excitatory and Inhibitory Neurons in Layer 2/3 of
924 Mouse Barrel Cortex." *Journal of Neurophysiology* 107 (11): 3116–34.
925 https://doi.org/10.1152/jn.00917.2011.
926 Bannai, Hiroko, Sabine Lévi, Claude Schweizer, Takafumi Inoue, Thomas Launey, Victor
927 Racine, Jean-Baptiste Sibarita, Katsuhiko Mikoshiba, and Antoine Triller. 2009.
928 "Activity-Dependent Tuning of Inhibitory Neurotransmission Based on GABAAR
929 Diffusion Dynamics." *Neuron* 62 (5): 670–82.
930 https://doi.org/10.1016/j.neuron.2009.04.023.
931 Battaglia, Sereina, Marianne Renner, Marion Russeau, Etienne Côme, Shiva K. Tyagarajan,

and Sabine Lévi. 2018. "Activity-Dependent Inhibitory Synapse Scaling Is Determined by Gephyrin Phosphorylation and Subsequent Regulation of GABAA Receptor Diffusion." *ENeuro* 5 (1): ENEURO.0203-17.2017. https://doi.org/10.1523/ENEURO.0203-17.2017.

Choquet, Daniel, and Antoine Triller. 2013. "The Dynamic Synapse." *Neuron* 80 (3): 691–703. https://doi.org/10.1016/J.NEURON.2013.10.013.

Crochet, Sylvain, James F.A. Poulet, Yves Kremer, and Carl C.H. Petersen. 2011. "Synaptic Mechanisms Underlying Sparse Coding of Active Touch." *Neuron* 69 (6): 1160–75. https://doi.org/10.1016/j.neuron.2011.02.022.

Dejanovic, Borislav, and Guenter Schwarz. 2014. "Brief Communications Neuronal Nitric Oxide Synthase-Dependent S-Nitrosylation of Gephyrin Regulates Gephyrin Clustering at GABAergic Synapses." https://doi.org/10.1523/JNEUROSCI.0531-14.2014.

Dejanovic, Borislav, Marcus Semtner, Silvia Ebert, Tobias Lamkemeyer, Franziska Neuser, Bernhard Lüscher, Jochen C. Meier, and Guenter Schwarz. 2014. "Palmitoylation of Gephyrin Controls Receptor Clustering and Plasticity of GABAergic Synapses." Edited by Matthew B.Dalva. *PLoS Biology* 12 (7): e1001908. https://doi.org/10.1371/journal.pbio.1001908.

El-Boustani, Sami, B. Semihcan Sermet, Georgios Foustoukos, Tess B. Oram, Ofer Yizhar, and Carl C.H. Petersen. 2020. "Anatomically and Functionally Distinct Thalamocortical Inputs to Primary and Secondary Mouse Whisker Somatosensory Cortices." *Nature Communications 2020 11:1* 11 (1): 1–12. https://doi.org/10.1038/s41467-020-17087-7.

Feldman, Daniel E., and Michael Brecht. 2005. "Map Plasticity in Somatosensory Cortex." *Science*. MIT Press. https://doi.org/10.1126/science.1115807.

Flores, Carmen E., Irina Nikonenko, Pablo Mendez, Jean-Marc Fritschy, Shiva K. Tyagarajan, and Dominique Muller. 2015. "Activity-Dependent Inhibitory Synapse

957 Remodeling through Gephyrin Phosphorylation." *Proceedings of the National Academy*
958 *of Sciences* 112 (1): E65–72. https://doi.org/10.1073/pnas.1411170112.
959 Freund, Tamás F. 2003. "Interneuron Diversity Series: Rhythm and Mood in Perisomatic
960 Inhibition." *Trends in Neurosciences* 26 (9): 489–95. https://doi.org/10.1016/S0166-
961 2236(03)00227-3.
962 Fritschy, Jean-Marc, and Hanns Mohler. 1995. "GABAA-receptor Heterogeneity in the Adult
963 Rat Brain: Differential Regional and Cellular Distribution of Seven Major Subunits."
964 *Journal of Comparative Neurology* 359 (1): 154–94.
965 https://doi.org/10.1002/cne.903590111.
966 Fritschy, Jean Marc, and Patrizia Panzanelli. 2014. "GABAA Receptors and Plasticity of
967 Inhibitory Neurotransmission in the Central Nervous System." *European Journal of*
968 *Neuroscience* 39 (11): 1845–65. https://doi.org/10.1111/ejn.12534.
969 Fritschy, Jean Marc, Patrizia Panzanelli, and Shiva K. Tyagarajan. 2012. "Molecular and
970 Functional Heterogeneity of GABAergic Synapses." *Cellular and Molecular Life*
971 *Sciences* 69 (15): 2485–99. https://doi.org/10.1007/s00018-012-0926-4.
972 Gao, Yudong, and Scott A. Heldt. 2016. "Enrichment of GABAA Receptor α-Subunits on the
973 Axonal Initial Segment Shows Regional Differences." *Frontiers in Cellular*
974 *Neuroscience* 10 (March): 39. https://doi.org/10.3389/fncel.2016.00039.
975 Gentet, Luc J., Michael Avermann, Ferenc Matyas, Jochen F. Staiger, and Carl C.H.
976 Petersen. 2010. "Membrane Potential Dynamics of GABAergic Neurons in the Barrel
977 Cortex of Behaving Mice." *Neuron* 65 (3): 422–35.
978 https://doi.org/10.1016/J.NEURON.2010.01.006.
979 Gentet, Luc J, Yves Kremer, Hiroki Taniguchi, Z Josh Huang, Jochen F Staiger, and Carl C
980 H Petersen. 2012. "Unique Functional Properties of Somatostatin-Expressing
981 GABAergic Neurons in Mouse Barrel Cortex." *Nature Neuroscience* 15 (4): 607–12.

https://doi.org/10.1038/nn.3051.

Ghosh, Himanish, Luca Auguadri, Sereina Battaglia, Zahra Simone Thirouin, Khaled Zemoura, Simon Messner, Mario A. Acuña, et al. 2016. "Several Posttranslational Modifications Act in Concert to Regulate Gephyrin Scaffolding and GABAergic Transmission." *Nature Communications* 7: 1–16. https://doi.org/10.1038/ncomms13365.

Groot, Clairede, Amalia Floriou-Servou, Yuan Chen Tsai, Simon Früh, Manuela Kohler, Georgia Parkin, Cornelia Schwerdel, et al. 2017. "RhoGEF9 Splice Isoforms Influence Neuronal Maturation and Synapse Formation Downstream of A2 GABAAreceptors." *PLoS Genetics* 13 (10): 1–27. https://doi.org/10.1371/journal.pgen.1007073.

Hines, Rochelle M., Hans Michael Maric, Dustin J. Hines, Amit Modgil, Patrizia Panzanelli, Yasuko Nakamura, Anna J. Nathanson, et al. 2018. "Developmental Seizures and Mortality Result from Reducing GABAA Receptor A2-Subunit Interaction with Collybistin." *Nature Communications* 9 (1): 1–15. https://doi.org/10.1038/s41467-018-05481-1.

Hofer, Sonja B., Ho Ko, Bruno Pichler, Joshua Vogelstein, Hana Ros, Hongkui Zeng, Ed Lein, Nicholas A.Lesica, andThomas D.Mrsic-Flogel. 2011. "Differential Connectivity and Response Dynamics of Excitatory and Inhibitory Neurons in Visual Cortex." *Nature Neuroscience* 14 (8): 1045–52. https://doi.org/10.1038/nn.2876.

Holmgren, Carl, Tibor Harkany, Björn Svennenfors, and Yuri Zilberter. 2003. "Pyramidal Cell Communication within Local Networks in Layer 2/3 of Rat Neocortex." *Journal of Physiology* 551 (1): 139–53. https://doi.org/10.1113/jphysiol.2003.044784.

Kapfer, Christoph, Lindsey L Glickfeld, Bassam V Atallah, and Massimo Scanziani. 2007. "Supralinear Increase of Recurrent Inhibition during Sparse Activity in the Somatosensory Cortex." *Nature Neuroscience* 10 (6): 743–53. https://doi.org/10.1038/nn1909.

1007 Kerti-Szigeti, Katalin, and Zoltan Nusser. 2016. “Similar GABAA Receptor Subunit
1008 Composition in Somatic and Axon Initial Segment Synapses of Hippocampal Pyramidal
1009 Cells.” *ELife* 5 (AUGUST). https://doi.org/10.7554/eLife.18426.001.
1010 Kim, Ji Yoen, Ryan T. Ash, Carolina Ceballos-Diaz, Yona Levites, Todd E. Golde, Stelios
1011 M. Smirnakis, and Joanna L. Jankowsky. 2013. “Viral Transduction of the Neonatal
1012 Brain Delivers Controllable Genetic Mosaicism for Visualising and Manipulating
1013 Neuronal Circuits in Vivo.” *European Journal of Neuroscience* 37 (8): 1203–20.
1014 https://doi.org/10.1111/ejn.12126.
1015 Koester, Christina, Uwe Rudolph, Tatjana Haenggi, Aurélie Papilloud, Jean-Marc Fritschy,
1016 and Florence Crestani. 2013. “Dissecting the Role of Diazepam-Sensitive γ-
1017 Aminobutyric Acid Type A Receptors in Defensive Behavioral Reactivity to Mild
1018 Threat.” *Pharmacology Biochemistry and Behavior* 103 (3): 541–49.
1019 https://doi.org/10.1016/J.PBB.2012.10.004.
1020 Kralic, Jason E., Corinne Sidler, Franziska Pakpan, Gregg E. Homanics, A. Leslie Morrow,
1021 and Jean Marc Fritschy. 2006. “Compensatory Alteration of Inhibitory Synaptic Circuits
1022 in Cerebellum and Thalamus of γ-Aminobutyric Acid Type A Receptor A1 Subunit
1023 Knockout Mice.” *Journal of Comparative Neurology* 495 (4): 408–21.
1024 https://doi.org/10.1002/cne.20866.
1025 Kuhse, Jochen, Heba Kalbouneh, Andrea Schlicksupp, Susanne Mükusch, Ralph Nawrotzki,
1026 and Joachim Kirsch. 2012. “Phosphorylation of Gephyrin in Hippocampal Neurons by
1027 Cyclin-Dependent Kinase CDK5 at Ser-270 Is Dependent on Collybistin.” *The Journal*
1028 *of Biological Chemistry* 287 (37): 30952–66. https://doi.org/10.1074/jbc.M112.349597.
1029 Lefort, Sandrine, Christian Tomm, J.-C.Floyd Sarria, and Carl C.H. Petersen. 2009. “The
1030 Excitatory Neuronal Network of the C2 Barrel Column in Mouse Primary
1031 Somatosensory Cortex.” *Neuron* 61 (2): 301–16.

https://doi.org/10.1016/j.neuron.2008.12.020.

Margolis, David J., Henry Lütcke, Kristina Schulz, Florent Haiss, Bruno Weber, Sebastian Kügler, Mazahir T. Hasan, and Fritjof Helmchen. 2012. "Reorganization of Cortical Population Activity Imaged throughout Long-Term Sensory Deprivation." *Nature Neuroscience* 15 (11): 1539–46. https://doi.org/10.1038/nn.3240.

Mayrhofer, Johannes M., Florent Haiss, Fritjof Helmchen, and Bruno Weber. 2015. "Sparse, Reliable, and Long-Term Stable Representation of Periodic Whisker Deflections in the Mouse Barrel Cortex." *NeuroImage* 115 (July): 52–63. https://doi.org/10.1016/J.NEUROIMAGE.2015.04.045.

Moretto Zita, M., Ivan Marchionni, Elisa Bottos, Massimo Righi, Giannino Del Sal, Enrico Cherubini, and Paola Zacchi. 2007. "Post-Phosphorylation Prolyl Isomerisation of Gephyrin Represents a Mechanism to Modulate Glycine Receptors Function." *EMBO Journal* 26 (7): 1761–71. https://doi.org/10.1038/sj.emboj.7601625.

Muir, James, and Josef T.Kittler. 2014. "Plasticity of GABAA Receptor Diffusion Dynamics at the Axon Initial Segment." *Frontiers in Cellular Neuroscience* 8 (June): 151. https://doi.org/10.3389/fncel.2014.00151.

Nguyen, Quynh Anh, and Roger A.Nicoll. 2018. "The GABAA Receptor β Subunit Is Required for Inhibitory Transmission." *Neuron* 98 (4): 718-725.e3. https://doi.org/10.1016/j.neuron.2018.03.046.

Nusser, Z, W Sieghart, D Benke, J M Fritschy, and P Somogyi. 1996. "Differential Synaptic Localization of Two Major Gamma-Aminobutyric Acid Type A Receptor Alpha Subunits on Hippocampal Pyramidal Cells." *Proceedings of the National Academy of Sciences of the United States of America* 93 (21): 11939–44. https://doi.org/10.1073/pnas.93.21.11939.

Nyíri, Gábor, Tamás F. Freund, and Péter Somogyi. 2001. "Input-Dependent Synaptic

1057 Targeting of A2-Subunit-Containing GABAA Receptors in Synapses of Hippocampal
1058 Pyramidal Cells of the Rat." *European Journal of Neuroscience* 13 (3): 428–42.
1059 https://doi.org/10.1046/j.1460-9568.2001.01407.x.
1060 Ohkura, Masamichi, Takuya Sasaki, Chiaki Kobayashi, Yuji Ikegaya, and Junichi Nakai.
1061 2012. "An Improved Genetically Encoded Red Fluorescent Ca2+ Indicator for Detecting
1062 Optically Evoked Action Potentials." *PLoS ONE* 7 (7).
1063 https://doi.org/10.1371/journal.pone.0039933.
1064 Panzanelli, Patrizia, Benjamin G. Gunn, Monika C. Schlatter, Dietmar Benke, Shiva K.
1065 Tyagarajan, Peter Scheiffele, Delia Belelli, Jeremy J. Lambert, Uw eRudolph, and Jean
1066 Marc Fritschy. 2011. "Distinct Mechanisms Regulate GABA A Receptor and Gephyrin
1067 Clustering at Perisomatic and Axo-Axonic Synapses on CA1 Pyramidal Cells." *Journal*
1068 *of Physiology* 589 (20): 4959–80. https://doi.org/10.1113/jphysiol.2011.216028.
1069 Petersen, Carl C. H. 2019. "Sensorimotor Processing in the Rodent Barrel Cortex." *Nature*
1070 *Reviews Neuroscience*, July, 1–14. https://doi.org/10.1038/s41583-019-0200-y.
1071 Petersen, Carl C.H. 2014. "Cell-Type Specific Function of GABAergic Neurons in Layers 2
1072 and 3 of Mouse Barrel Cortex." *Current Opinion in Neurobiology*.
1073 https://doi.org/10.1016/j.conb.2013.10.004.
1074 Rajgor, Dipen, Alicia M. Purkey, Jennifer L. Sanderson, Theresa M.Welle, Joshua D.Garcia,
1075 Mark L. Dell'Acqua, and Katharine R. Smith. 2020. "Local MiRNA-Dependent
1076 Translational Control of GABAAR Synthesis during Inhibitory Long-Term
1077 Potentiation." *Cell Reports* 31 (12): 107785.
1078 https://doi.org/10.1016/j.celrep.2020.107785.
1079 Sommeijer, Jean Pierre, Mehran Ahmadlou, M. Hadi Saiepour, Koen Seignette, Rogier Min,
1080 J. Alexander Heimel, and Christiaan N. Levelt. 2017. "Thalamic Inhibition Regulates
1081 Critical-Period Plasticity in Visual Cortex and Thalamus." *Nature Neuroscience 2017*

20:12 20 (12): 1715–21. https://doi.org/10.1038/s41593-017-0002-3.

Stobart, Jillian L., Kim David Ferrari, Matthew J.P. Barrett, Chaim Glück, Michael J. Stobart, Marc Zuend, and Bruno Weber. 2018. "Cortical Circuit Activity Evokes Rapid Astrocyte Calcium Signals on a Similar Timescale to Neurons." *Neuron* 98 (4): 726-735.e4. https://doi.org/10.1016/j.neuron.2018.03.050.

Szabadics, János, Csaba Varga, Gábor Molnár, Szabolcs Oláh, Pál Barzó, and Gábor Tamás. 2006. "Excitatory Effect of GABAergic Axo-Axonic Cells in Cortical Microcircuits." *Science* 311 (5758): 233–35. https://doi.org/10.1126/science.1121325.

Turrigiano, Gina G., and Sacha B. Nelson. 2000. "Hebb and Homeostasis in Neuronal Plasticity." *Current Opinion in Neurobiology*. Current Biology Ltd. https://doi.org/10.1016/S0959-4388(00)00091-X.

Tyagarajan, Shiva K., and Jean Marc Fritschy. 2014. "Gephyrin: A Master Regulator of Neuronal Function?" *Nature Reviews Neuroscience* 15 (3): 141–56. https://doi.org/10.1038/nrn3670.

Vicini, S, C Ferguson, K Prybylowski, J Kralic, A L Morrow, and G E Homanics. 2001. "GABA(A) Receptor Alpha1 Subunit Deletion Prevents Developmental Changes of Inhibitory Synaptic Currents in Cerebellar Neurons." *The Journal of Neuroscience : The Official Journal of the Society for Neuroscience* 21 (9): 3009–16. https://doi.org/10.1523/JNEUROSCI.21-09-03009.2001.

Figure legends

Figure 1. $GABA_AR$ subunit expression changes after altered sensory input. (A) An overview of bilateral viral injections into lateral ventricles at P0, followed by stimulation (Stim) or whisker trimming (Trim) protocol for 1 week prior to morphology analysis on individual pyramidal neurons. Trim group, the whiskers were trimmed bilaterally every day to the same

length as the facial hair. The Stim group received daily 1 minute of large angle whisker deflection bilaterally. (B) Representative images of L2/3 pyramidal neurons in barrel cortex from control, trim and stim groups expressing α1-$GABA_AR$ subunit. (C) Representative images of L2/3 pyramidal neurons in barrel cortex from control, trim and stim groups expressing α2-$GABA_AR$ subunit. (D-E) Quantification of cluster analysis of density and size for α1-$GABA_AR$ from N=4 mice for control and trim groups, N=5 for Stim group. (F-G) Quantification of cluster analysis of density and size for α2-$GABA_AR$. In total, 10-15 neurons were imaged per mouse and data points represent average of individual animals. Statistics: One-way ANOVA, with Bonferroni post hoc test. Error bar: standard deviation. *p≤0.05, **p≤0.01, ***p≤0.001.

Figure 2. L2/3 pyramidal neuron activity changes in *Gabra1* KO mice. (A) Overview of virus injection protocol for *in vivo* 2-photon imaging. AAV6-CaMKIIa-RCaMP virus was injected into the barrel cortex. After 1-month, the mice were subjected to a series of imaging composed of spontaneous and whisker stimulation imaging sessions, and each session was composed of forty 15-second trials (with 3-second inter-trial interval). Each whisker stimulation trial consisted of 1 second of 90 Hz whisker stimulation after 2.5 seconds of baseline. **(B)** Average trace example of spontaneous and whisker stimulation imaging sessions. Grey bar: whisker stimulation. Standard deviations are shown in lighter colors under the example trace. **(C-C'')** Average Ca^{2+} transient amplitude, duration, and number of events in whisker stimulation trials in density plots and bar graphs (insets). The average was obtained from all imaging sessions for individual neurons (N=459 neurons from 5 *Gabra1* KO mice, N=418 neurons from 4 WT mice). **(D)** Proportions of high and lower responding cells were selected based on ~10% of high Ca^{2+} transient amplitude versus rest. **(E-E'')** Quantification of amplitude, duration and the number of events between the high responders of WT and *Gabra1*

KO. Statistics: linear mixed-effects models and Tukey post hoc tests. All bar graphs are represented as mean ± SEM. *p≤0.05, **p≤0.01, ***p≤0.001. **(F)** Miniature IPSC (mIPSC) traces were recorded from *Gabra1* WT and KO littermates L2/3 barrel cortex. Average: solid black (WT) and red (KO). All traces are shown in grey. **(G)** mIPSC amplitude **(H)** mIPSC inter-event interval (IEI) from *Gabra1* WT and KO are shown. Cumulative distribution is plotted. Inset: each dot represents a recorded cell (all events averaged). **(I)** Averaged rise time **(J)** and decay time of mIPSC. Each dot represents a recorded cell. Total 3 WT (7 cells) and 3 KO (10 cells). Statistics: Welch's t-test, mean ± SEM. *p≤0.05, **p≤0.01, ***p≤0.001.

Figure 3. L2/3 pyramidal neuron activity change in *Gabra2* KO mice. (A) Average trace from an example of spontaneous and whisker stimulation imaging session. Grey bar: whisker stimulation. Standard deviations are shown in lighter colors below the example trace. **(B-B')** Average Ca^{2+} transient amplitude, duration and number of events in whisker stimulation trials in density plots and bar graphs (insets). N=370 neurons from 4 *Gabra2* KO mice, N=307 neurons from 3 WT mice. **(C)** Proportions of high and lower responding cells selected based on ~10% of high Ca^{2+} transient amplitude versus rest. **(D-D'')** Quantification of amplitude, duration and the number of events measured both high responders in WT and *Gabra2* KO. Statistics: linear mixed-effects models and Tukey post hoc tests. All bar graphs are represented as mean ± SEM. *p≤0.05, **p≤0.01, ***p≤0.001. **(E)** Miniature IPSC traces were recorded from *Gabra2* WT and KO L2/3 barrel cortex. Average: solid black (WT) and red (KO). All traces are shown in grey. **(F)** Amplitude **(G)** and IEI of mIPSC from *Gabra2* WT and KO littermates. Cumulative distribution plotted. Inset: each dot represents a recorded cell (all events averaged). **(H)** Averaged rise time **(I)** and decay time of mIPSC. Each dot represents a recorded cell. Total 3 WT (8 cells) and 4 KO (17 cells). Statistics: Welch's t-test, mean ± SEM. *p≤0.05, **p≤0.01, ***p≤0.001.

Figure 4. Cell-autonomous contribution of α1-GABA$_A$R and α2-GABA$_A$R in L2/3 pyramidal neuron whisker derived activity. (A) Method illustration. The *Gabra1$^{flox/flox}$* or *Gabra2$^{flox/flox}$* mice were injected with AAV6-CaMKIIα-RCaMP (control) or combined with AAV6-CaMKIIα-eGFP-Cre. The cell population received the viral mixture RCaMP and Cre, named Cre-positive (red cells with green nuclei). Right panel: representative picture from a field of view expressing RCaMP and Cre. White arrowhead: example of cre-positive cells. **(B-B'')** Spontaneous and stimulation-induced Ca^{2+} transient amplitude, duration, and the number of events for control and Cre-positive RCaMP-expressing neurons from *Gabra1$^{flox/flox}$* mice. N=123 control neurons and N=47 cre-positive neurons from 2-4 mice per group. **(C-C'')** Spontaneous and stimulation-induced Ca^{2+} transient amplitude, duration, and the number of events for control and Cre-positive RCaMP-expressing neurons from *Gabra2$^{flox/flox}$* mice. N=150 control neurons and N=262 Cre-positive RCaMP-neurons from 3-5 mice per group. **(D-D')** Proportions of high- and lower-responding cells selected based on 90th percentiles of the control group for spontaneous and stimulation-induced Ca^{2+} transient amplitude in *Gabra1$^{flox/flox}$* **(D)** and *Gabra2$^{flox/flox}$* mice **(D')**. The same amplitude cut-off levels are then applied to the control and Cre-positive neurons of *Gabra1$^{flox/flox}$* and *Gabra2$^{flox/flox}$* mice. Statistics: linear mixed-effects models and Tukey post-hoc tests. All bar graphs are represented as mean ± SEM. *p≤0.05, **p≤0.01, ***p≤0.001, the stars indicate the significance of the comparison between spontaneous and stimulation. The significance of cross-group comparisons are indicated in the text.

Figure 5. GABAergic neurotransmission changes in gephyrin-mutant-expressing L2/3 pyramidal neurons. (A) An illustration of different gephyrin mutations used in the study, along with the signaling pathways that are affected by the mutated residue. The gephyrin-K148R (SUMO1 conjugation site mutant) facilitates scaffolding. The gephyrin-S303A and

S305A (PKA and CaMKIIα phospho-null mutant) hampers NMDA receptor activity-induced scaling at GABAergic postsynaptic sites. The gephyrin-DN (lacks part of E domain) disrupts endogenous gephyrin scaffolds in neurons. **(B)** Representative images of neuron co-expressing RCaMP and eGFP-gephyrin variants after injection of AAV in L2/3 barrel cortex *in vivo*. The following combination of viruses were injected to the barrel cortex (same combination used in 2P Ca^{2+} imaging): AAV6-hSyn1-flex-gephyrin mutant, AAV6-CaMKIIa-$CreER^{T2}$, AAV6-CaMKIIa-RCaMP1.07. All brain sections were stained for CaMKIIα and eGFP. **(C)** Example traces from L2/3 pyramidal cells expressing gephyrin variants or GFP control. Colored traces: averaged current from one neuron. Grey traces: all events measured from one neuron. **(D)** Miniature inhibitory postsynaptic currents (mIPSCs) amplitude and the inter-event interval (IEI) in L2/3 pyramidal neurons expressing individual gephyrin variants. Statistics: eGFP, n=23; K148R, n=13; gephyrin-DN, n=13; gephyrin-SSA, n=10 neurons, from 4-5 mice in each group. One-way ANOVA with Tukey post-hoc test. Bars: mean ± SEM. *p≤0.05, **p≤0.01, ***p≤0.001, ****p≤0.0001.

Figure 6. The expression of gephyrin mutants modulate L2/3 pyramidal neuron excitability differentially. (A) An overview of the viral infection *in vivo*. The control site (Area 1) received only AAV6-CaMKIIα-RCaMP1.07, while the experimental site (Area 2) received a combination of RCaMP/CaMKIIα-eGFP-Cre-gephyrin viruses. **(B)** Average trace examples from imaging sessions for whisker stimulation trials of both before and after gephyrin mutant expression. Grey bar: whisker stimulation. Lighter colors around the example trace are standard deviations. **(C-C'')** Average percentage changes after gephyrin-mutant expression for individual neurons are shown in bar graphs and the ratios are shown as violin plots to demonstrate the distribution differences in stimulation-induced Ca^{2+} transients. **(D)** Onset and decay time for before and after expression of the gephyrin mutants. eGFP, n=491 neurons;

gephyrin-K148R, n=308 neurons; gephyrin-SSA, n=249 neurons; gephyrin-DN, n=204 neurons. Statistics: linear mixed-effects models and Tukey post hoc tests. All bar graphs are represented as mean ± SEM. *p≤0.05, **p≤0.01, ***p≤0.001.

Figure 7. Interaction of gephyrin variants and α1- or α2-GABA$_A$R subtypes. The primary cortical neurons were transfected with eGFP-gephyrin WT, eGFP-gephyrin DN, eGFP-Gephyrin K148R or eGFP-gephyrin SSA mutant at 13 days in vitro (13 DIV) and stained for α1 and α2 subunit of GABA$_A$Rs at 20 DIV. (A) Example images of transfected neurons with gephyrin mutants. Scale bar: 25 μm. Lower panels: magnified images of selected dendrites (white box). White arrows: eGFP-gephyrin clusters without GABRA2 staining. (B) Cluster analysis was performed to show the density of colocalization of eGFP-gephyrin variants with α1-GABA$_A$Rs and α2-GABA$_A$Rs. eGFP-gephyrin DN was excluded from cluster analysis as the GFP signal was diffused. Statistics: One-way ANOVA, with Tukey post hoc test. *p≤0.05, **p≤0.01, ***p≤0.001.

Suppl. Figure 1. Spontaneous L2/3 pyramidal neuron activity in Gabra1 KO mice. (A) Field of view and ROI selection from RCaMP-expressing barrel cortex L2/3; (right panel) representative whole frame and individual traces from a whisker stimulation trial. **(B-B'')** Average Ca^{2+} transient amplitude, duration and number of events in spontaneous trials in density plots and bar graphs (insets). **(C-C')** Onset and decay times of Ca^{2+} transients in WT and *Gabra1* KO mice. The average was taken from all imaging sessions for individual neurons (N=459 neurons from 5 *Gabra1* KO mice, N=418 neurons from 4 WT mice). Statistics: linear mixed-effects models and Tukey post hoc tests. All bar graphs are represented as mean ± SEM. *p≤0.05, **p≤0.01, ***p≤0.001. **(D)** Immunohistochemistry of *Gabra1* WT and KO mice. Example images from L2/3 barrel cortex stained with VGAT, gephyrin and GABRA2 (α2)

subunit. Scale bar: 25 µm. **(E-E'''')** Quantification of cluster density analyses of VGAT, gephyrin and GABRA2, and their colocalization. Statistics: t-test. Error bar: standard deviation. *p≤0.05

Suppl. Figure 2. Spontaneous L2/3 pyramidal neuron activity in Gabra2 KO mice. (A) Field of view and ROI selection from virus infected barrel cortex L2/3; (right panel) representative whole frame and individual traces from 1 whisker stimulation trial. **(B-B'')** Average Ca^{2+} transient amplitude, duration and number of events in spontaneous trials in density plots and bar graphs (insets). **(C-C')** Onset and decay times of Ca^{2+} transients in WT and *Gabra2* KO mice. The average was taken from all imaging sessions for individual neurons (N=370 neurons from 4 *Gabra2* KO mice, N=307 neurons from 3 WT mice). Statistics: linear mixed-effects models and Tukey post hoc tests. All bar graphs are represented as mean ± SEM. *p≤0.05, **p≤0.01, ***p≤0.001. **(D)** Immunohistochemistry of *Gabra2* WT and KO mice. Example images from L2/3 barrel cortex stained with VGAT, gephyrin and GABRA1 (α1) subunit. Scale bar: 25 µm. **(E-E'''')** Quantification of cluster density analyses of VGAT, gephyrin and GABRA1, and their colocalization. Statistics: t-test (unpaired), mean ± SD.

Suppl. Figure 3. Changes in α1, α2, α3 $GABA_AR$ subunit expression in *Gabra1* and *Gabra2* KO mice. Whole cell protein lysates were prepared from barrel cortices of WT & *Gabra1* KO littermates **(A)** and WT and *Gabra2* KO littermates **(B)** (5 mice per group), and Western blot (WB) analysis was performed for gephyrin, α3, and α1 or α2. Protein level was normalised to total actin level for further quantification. **(A')** Quantification for gephyrin, α2, α3 protein expression changes between WT and *Gabra1* KO. **(B')** Quantification for gephyrin, α1, α3 protein expression changes between WT and *Gabra2* KO. Statistics: t-test (unpaired). All bar graphs are represented as mean ± SD. *p≤0.05, **p≤0.01, ***p≤0.001.

Suppl. Figure 4. Expression of RCaMP and eGFP_Cre and the neuronal activity in L2/3 pyramidal neuron *Gabra1*$^{flox/flox}$ and *Gabra2*$^{flox/flox}$ mice. (A, B) Immunohistochemistry from *Gabra1*$^{flox/flox}$ **(A)** and *Gabra2*$^{flox/flox}$ **(B)** mice received viral injections of AAV6-CaMKIIa-RCaMP1.07 and AAV8-CaMKIIα-eGFP-Cre. The brain sections were stained for GABRA1 or GABRA2 to validate the effects of conditional knockout for *Gabra1* and *Gabra2*, respectively, in L2/3 pyramidal neurons. Scale bar: 25 µm; 10 µm for zoom-in images. **(C, D)** Example images of the field of view and ROI selection for Cre-negative and Cre-positive RCaMP-expressing pyramidal neurons of *Gabra1*$^{flox/flox}$ **(C)** and *Gabra2*$^{flox/flox}$ **(D)** mice. Right panel: example traces in a trial with whisker stimulation. Grey bar: whisker stimulation period. **(E, F)** Density distribution of amplitude, duration and number of events for spontaneous and stimulation-induced Ca^{2+} transients from RCaMP control, Cre-negative cells expressing RCaMP, Cre-positive cells expressing RCaMP in *Gabra1*$^{flox/flox}$ **(E)** and in *Gabra2*$^{flox/flox}$ **(F)** mice.

Suppl. Figure 5. mIPSC and eIPSC recorded from gephyrin-DN-expressing L2/3 pyramidal neurons. (A) Normal distribution was plotted and tested using QQ plot and D'Agostino-Pearson test. **(B)** logIEI plot for control and gephyrin variants. Statistics: One-way or Brown-Forsythe and Welch One way ANOVA followed by Tukey's or Dunnet T3 multiple comparison tests. **(C)** Representative traces of evoked inhibitory postsynaptic currents (eIPSC) in a L2/3 pyramidal neuron of the barrel cortex of mice overexpressing control-eGFP and gephyrin-DN mutant. **(D)** Input/output curves and bar diagrams showing the eIPSC amplitude (pA) of L2/3 pyramidal neurons in GFP-expressing controls as compared to DN-expressing mutant mice for each stimulation paradigm (black, GFP: 4 mice, n=5; red, DN: 4 mice, n=4;

Two-way ANOVA, $F(8, 56) = 3.745$, $p = 0.0014$; Post hoc Sidak's multiple comparisons test, *$p \leq 0.05$). Data are reported as mean ± SEM.

Suppl. Figure 6. Percentage of L2/3 pyramidal neurons infected with different AAV virus. **(A)** Example images of barrel cortex L2/3 cells infected with AAV6-CaMKIIα-RCaMP1.07, AAV6-CaMKIIα-CreER^{T2} and AAV6-hSyn1-flex-gephyrin mutants. The neurons were stained for CaMKIIα and GFP. Scale bar: 20 µm. (B) Quantification of average expression of RCaMP-expressing neurons (72 %) and neurons co-expressing RCaMP and eGFP-gephyrin mutants (40 %) after normalization to total CaMKIIα-positive neurons.

Suppl. Figure 7. Spontaneous activity changes in L2/3 pyramidal neurons expressing gephyrin variants. (A-A'') Average percentage changes after gephyrin-mutant expression for individual neurons are shown in bar graphs and the ratio are shown in violin plots to demonstrate the distributions for spontaneous Ca^{2+} transients. **(B)** Proportions of high- and lower-responding neurons before and after gephyrin-mutant expression *in vivo* selected based on Ca^{2+} transient amplitude. **(C)** Proportions of high- and lower-responding neurons before and after gephyrin-mutant expression selected based on number of events. eGFP, n=491 neurons; gephyrin-K148R, n=308 neurons; gephyrin-SSA, n=249 neurons; gephyrin-DN, n=204 neurons. The numbers on the pie charts are rounded to the nearest integer. Statistics: linear mixed-effects models and Tukey post hoc tests. All bar graphs are represented as mean ± SEM. *$p \leq 0.05$, **$p \leq 0.01$, ***$p \leq 0.001$.

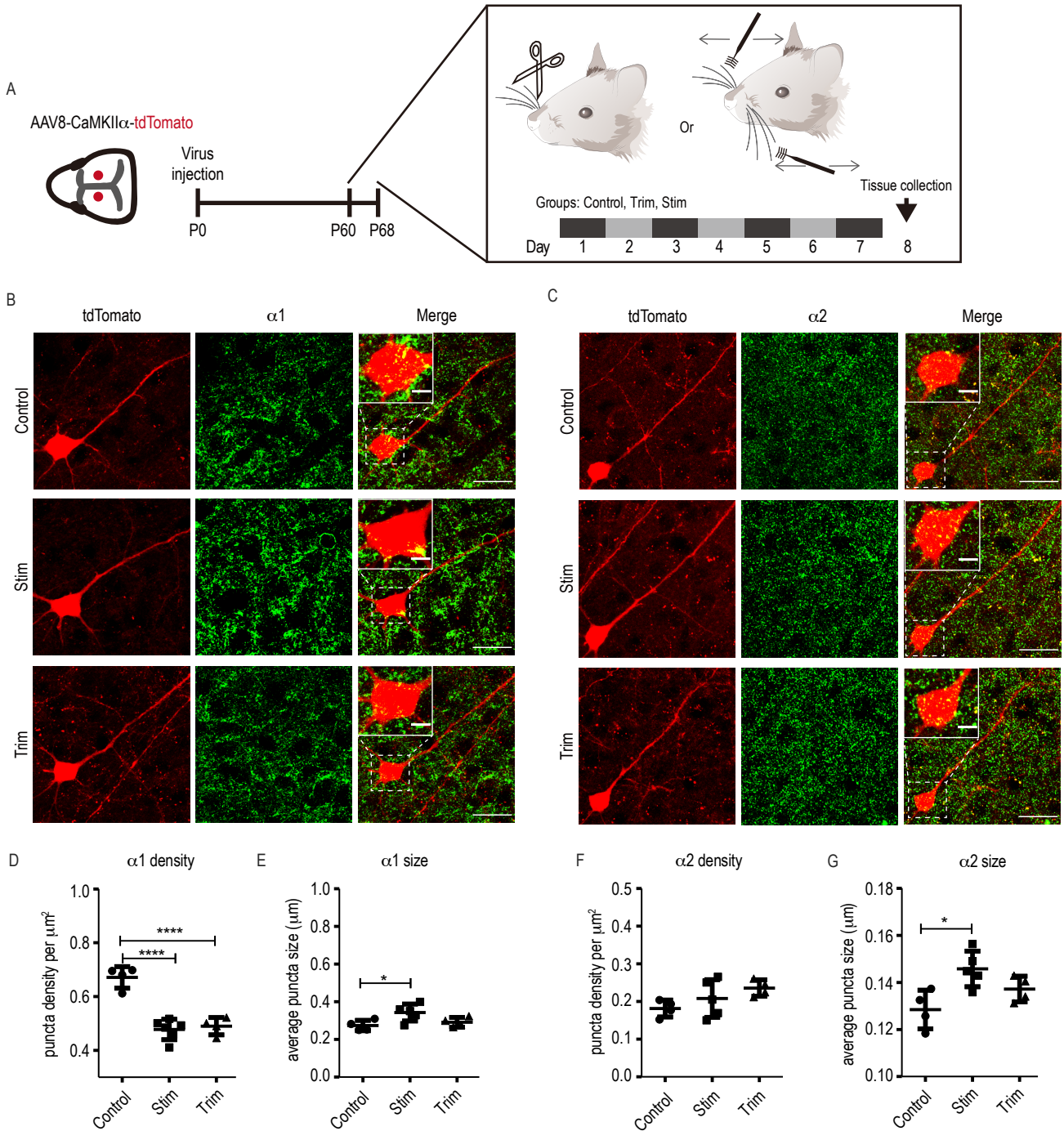

Figure 1.

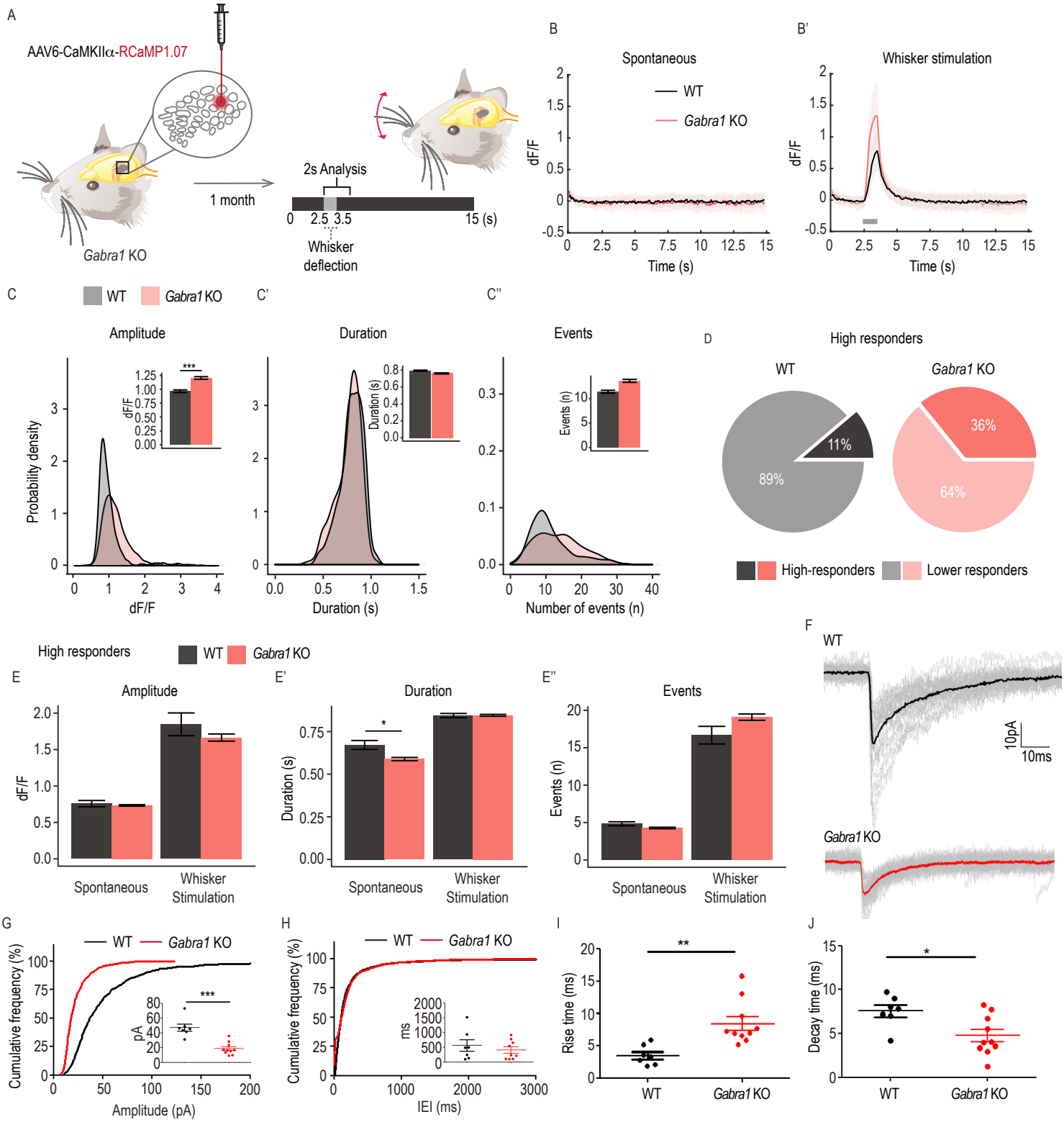

Figure 2.

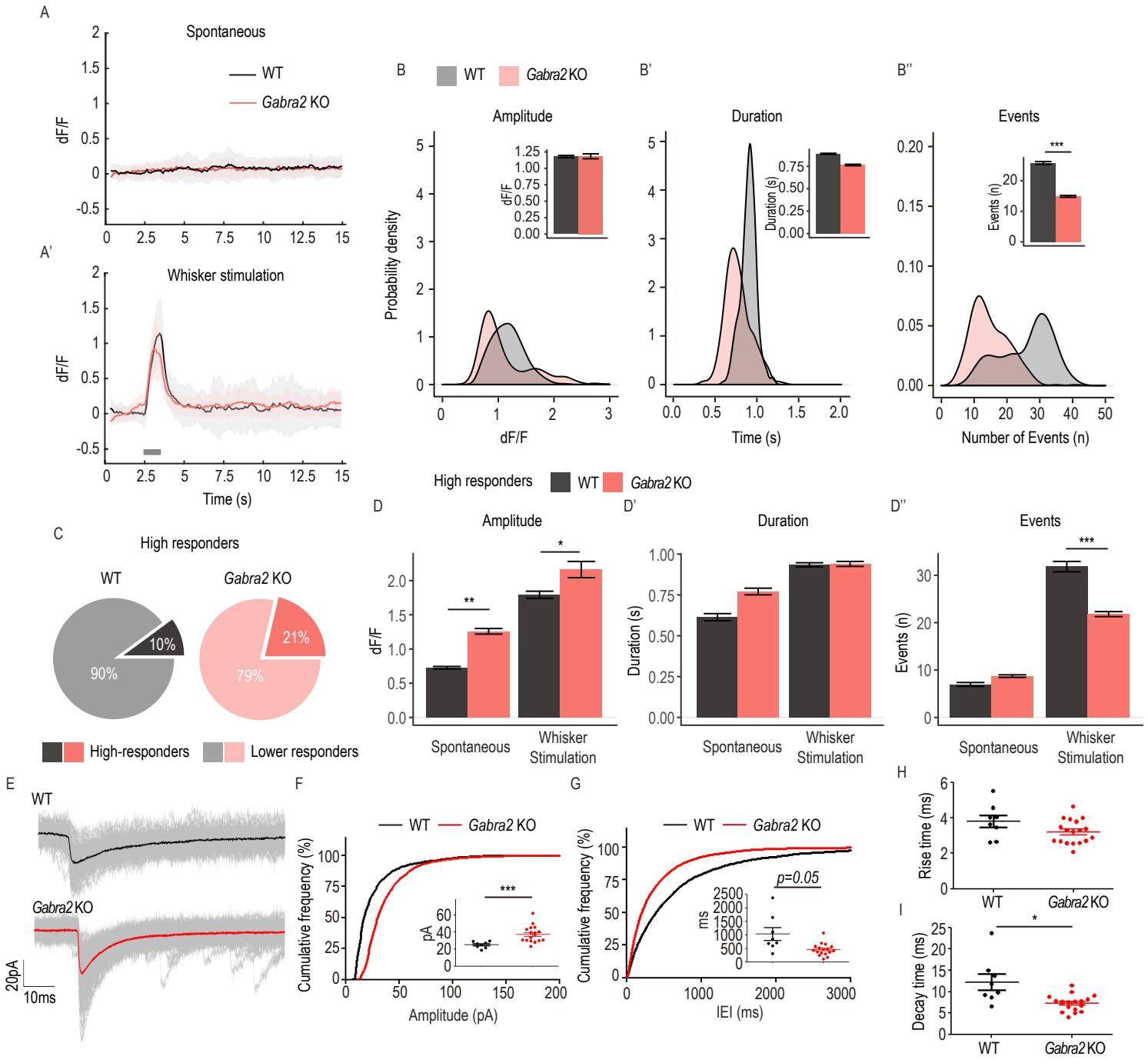

Figure 3.

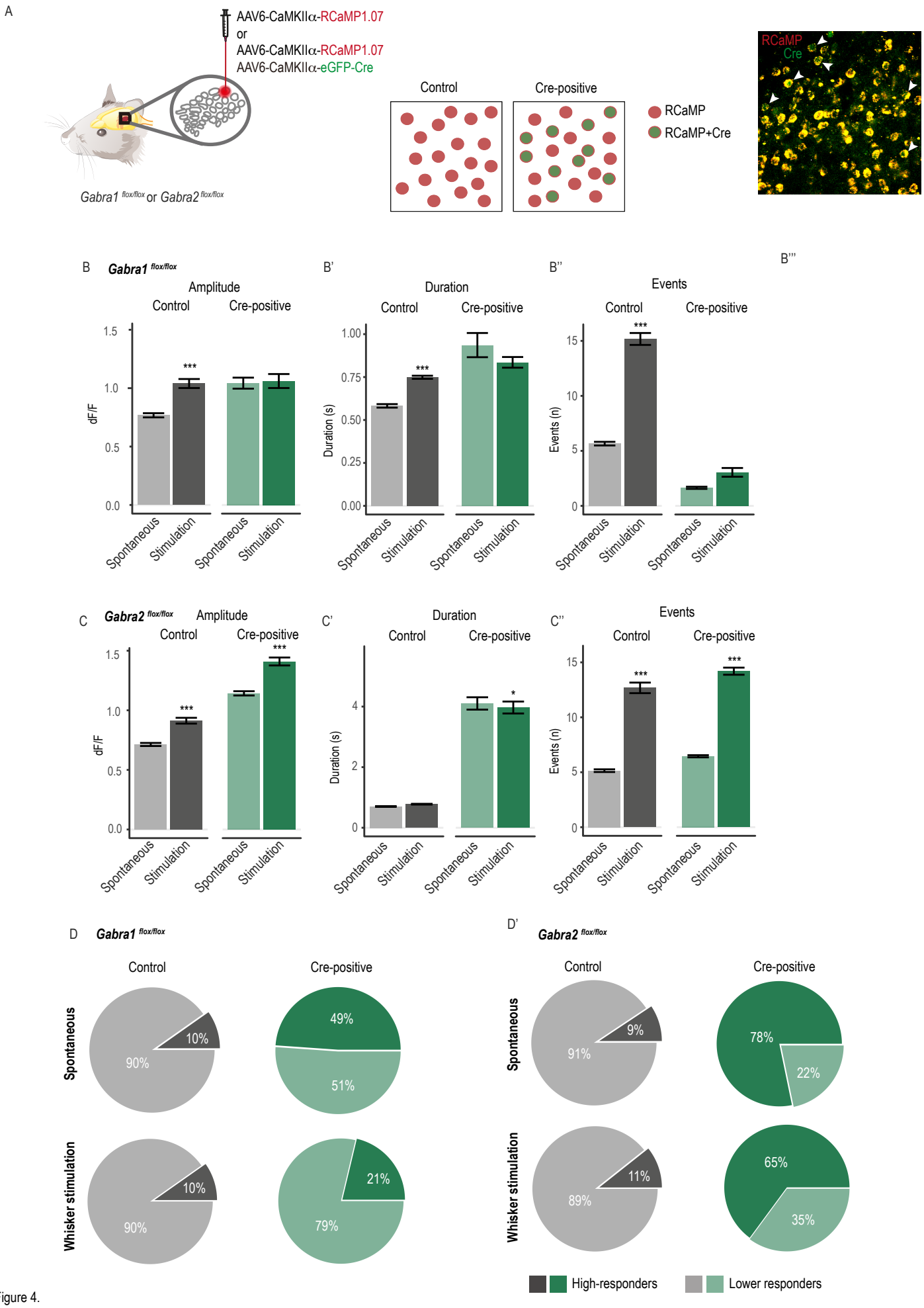

Figure 4.

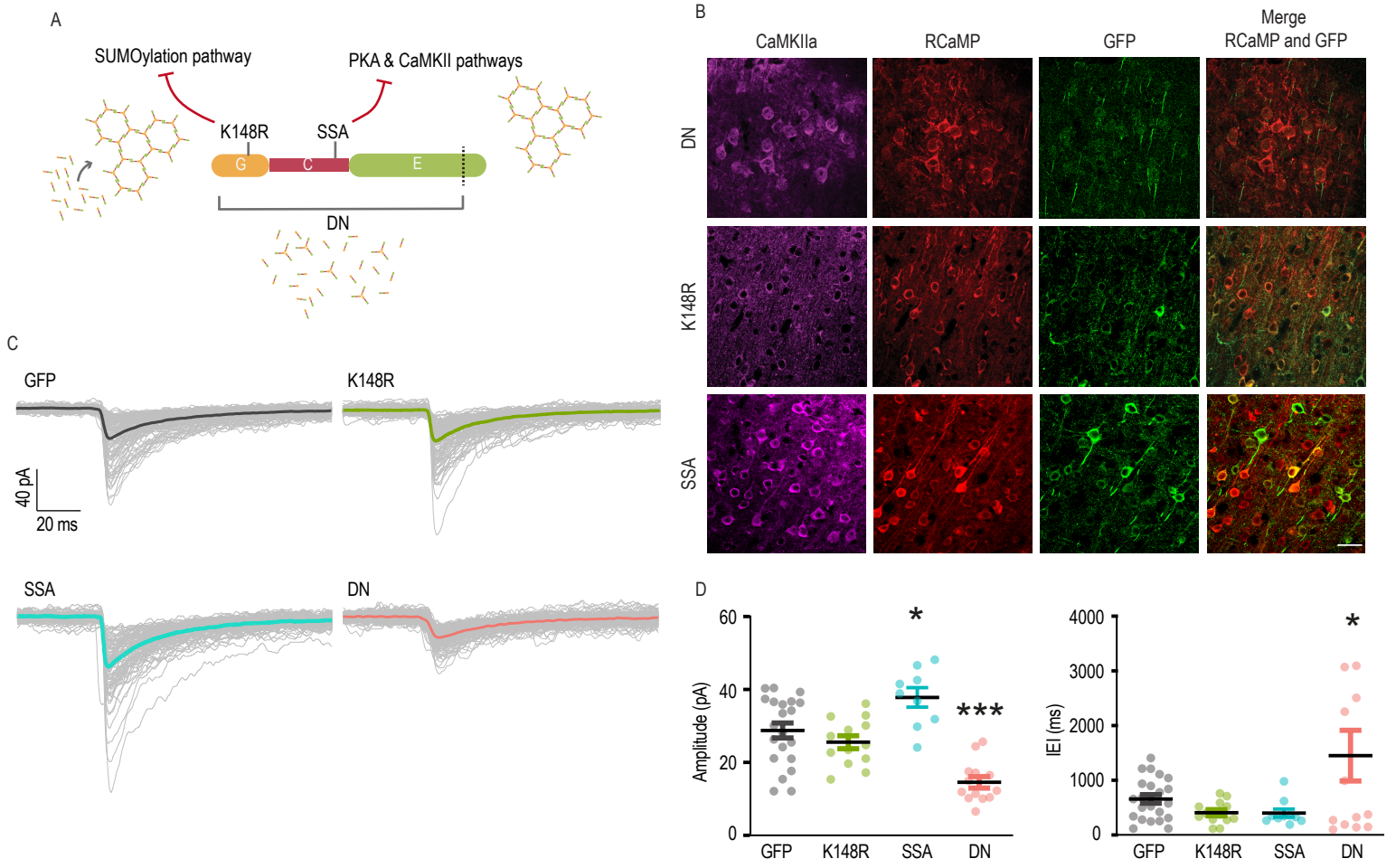

Figure 5.

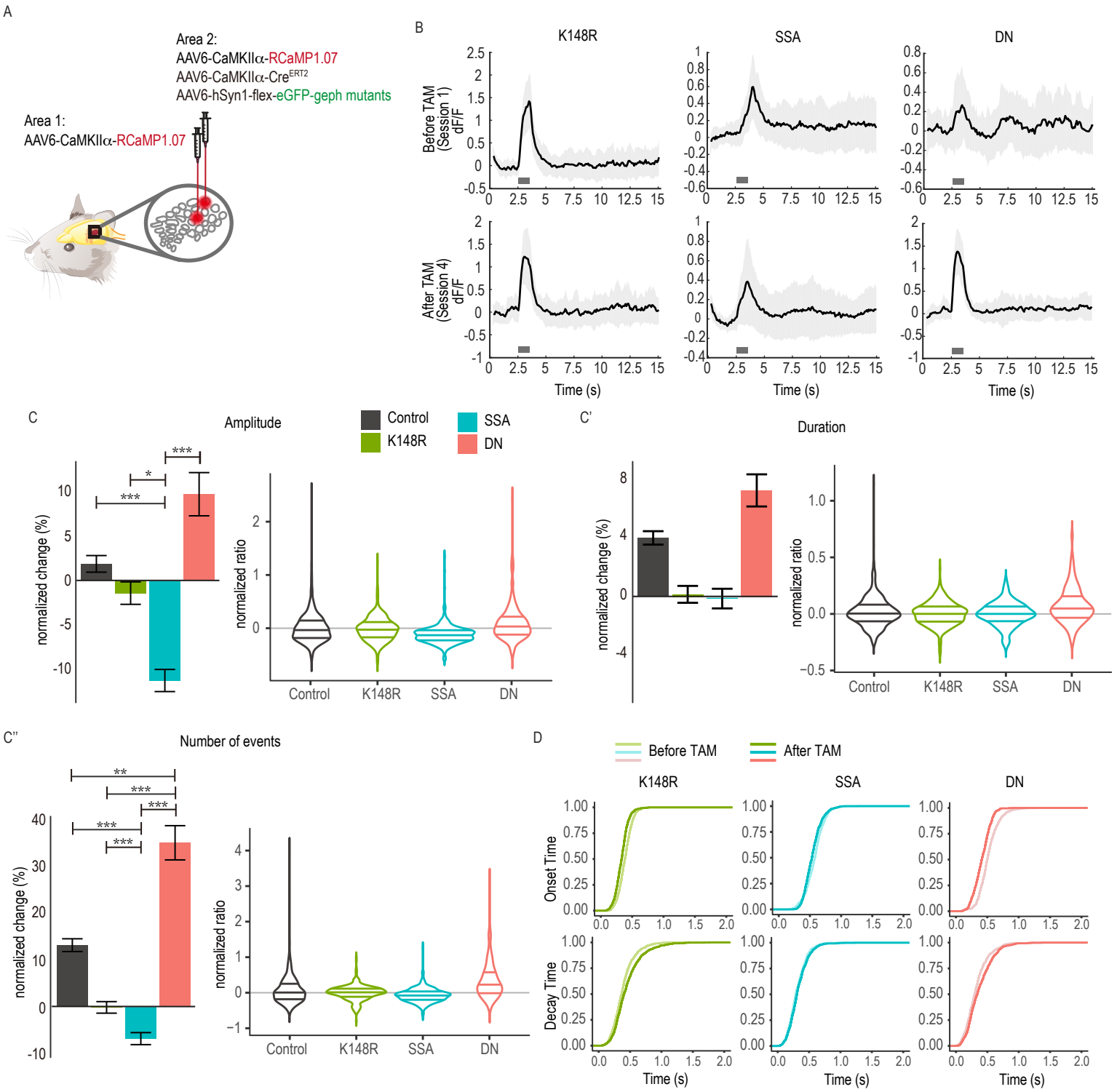

Figure 6.

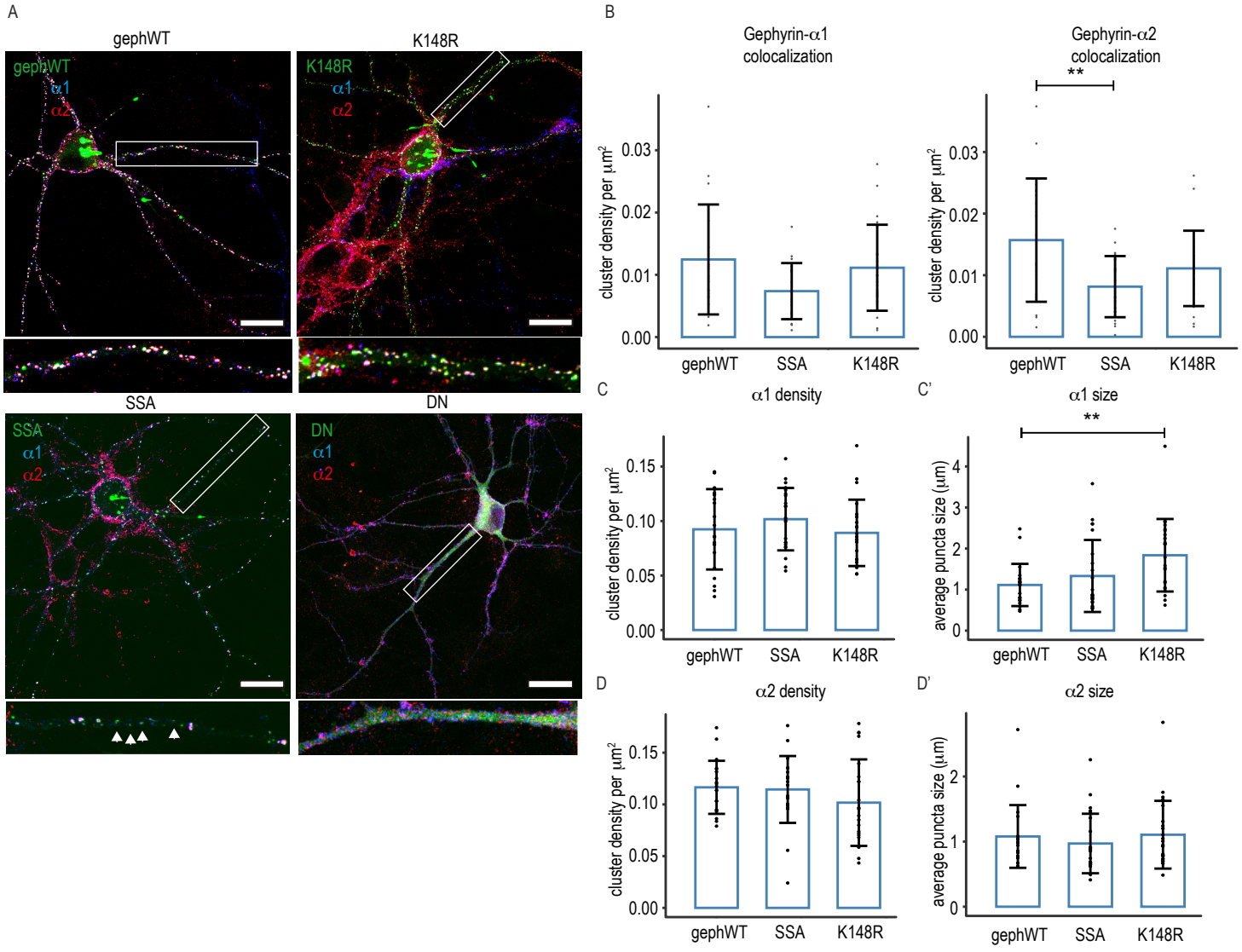

Figure 7.